Title	Development of composite functional tissue sheets using hiPSC-CMs and hADSCs to improve the cardiac function after myocardial infarction
Author(s)	Zhang, Jingbo; Li, Junjun; Qu, Xiang et al.
Citation	Bioactive Materials. 2024, 37, p. 533-548
Version Type	VoR
URL	https://hdl.handle.net/11094/98538
rights	This article is licensed under a Creative Commons Attribution-NonCommercial-NoDerivatives 4.0 International License.
Note	

Development of composite functional tissue sheets using hiPSC-CMs and hADSCs to improve the cardiac function after myocardial infarction

Jingbo Zhang [a], Junjun Li [a,b], Xiang Qu [c], Yuting Liu [a], Lifu Sun [a], Akima Harada [a], Ying Hua [a,1], Nagako Sougawa [a,d], Akiko Tabata [a], Li Liu [a,b,*], Shigeru Miyagawa [a,**]

[a] *Department of Cardiovascular Surgery, Osaka University Graduate School of Medicine, 2-2 Yamada-oka, Osaka, 565-0871, Japan*
[b] *Department of Applied Physics Osaka University, Osaka University, 2-2 Yamada-oka, Osaka, 565-0871, Japan*
[c] *Frontier of Regenerative Medicine, Osaka University Graduate School of Medicine, Suita, Osaka, 565-0871, Japan*
[d] *Department of Physiology, Osaka Dental University, 8-1 Kuzuha Hanazono-cho, Hirakata, 573-1121, Japan*

ARTICLE INFO

ABSTRACT

Human-induced pluripotent stem cell-derived cardiomyocytes (hiPSC-CMs) have been widely used in therapy of ischemic heart disease. However, there are still remaining issues that limit the therapeutic efficacy, such as immune rejection and low retention of hiPSC-CMs. Human adipose mesenchymal stromal cells (hADSCs) have been reported to be able to regulate the immune response, promote angiogenesis and promote the maturation of hiPSC-CMs. In this study, we co-cultured these two types of cells on fiber scaffold made of biodegradable poly (D, L-lactic-*co*-glycolic acid) (PLGA) polymer for several days to develop a composited 3D cardiac tissue sheet. As expected, the cells formed 231.00 $\pm$ 15.14 μm thickness tissue, with improved organization, alignment, ECM condition, contractile ability, and paracrine function compared to culture hiPSC-CMs only on PLGA fiber. Furthermore, the composited 3D cardiac tissue sheet significantly promoted the engraftment and survival after transplantation. The composited 3D cardiac tissue sheet also increased cardiac function, attenuated ventricular remodeling, decreased fibrosis, and enhanced angiogenesis in rat myocardial infarction model, indicating that this strategy wound be a promising therapeutic option in the clinical scenario.

1. Introduction

Currently, ischemic heart disease is the leading cause of death worldwide [1,2]. A major underlying pathophysiological issues in this disease is the constrained intrinsic regeneration capacity of the human myocardium after injury [3]. Although clinical treatments for myocardial infarction (MI) can achieve myocardial reperfusion, cardiomyocyte (CM) death caused by ischemia cannot be reversed [4].

Cell-based therapies, involving cell transplantation to compensate for cell loss, ameliorate non-specific inflammatory processes, rebuild the damaged tissue, and restore the organ function, have emerged as novel treatment strategies in regenerative medicine [5,6]. Various cell types have been explored as treatment options for ischemic heart disease leading to different outcomes in terms of therapeutic benefit [7,8]. Mesenchymal stem cells (MSCs) offer several advantages including easy

acquisition, low immunogenicity, and rapid proliferation, among them, hADSCs have been shown to improve cardiac contractility, reduce inflammation, adverse remodeling, and enhance vascularization via the secretion of several cytokines [9–15]. However, the cardiac functional recovery capacity of MSCs is limited owing to severe cell loss, uneven local distribution, and inability to restore the lost contractility necessary for proper electromechanical heart function. Several studies have demonstrated the potential of induced pluripotent stem cell-derived CMs (iPSC-CMs) to engraft and improve the performance of myocardium after MI [16–21]. Several iPSC-CMs are currently in the clinical trial phase [22]. However, iPSC-CMs exhibit limited retention and poor paracrine function after transplantation. Therefore, we aimed to simultaneously use these two cell types to develop composite tissues with the biomaterials as scaffold.

Poly (lactic-co-glycolic-acid) (PLGA) is a biodegradable and

biocompatible copolymer, which is widely used as a therapeutic device in drug delivery and tissue engineering applications. Its clinical use in humans has been approved by the U.S. Food and Drug Administration (FDA) [23,24]. In our previous studies, we have constructed 3D hiPSC-CM tissue sheets and 3D MSC tissue sheets using PLGA fiber scaffold [17,25]. Our tissue sheet technology based on PLGA fiber scaffold exhibits numerous advantages, including well-organized and thick tissue, abundant ECM deposition, enhanced secretion, simple construction methods, excellent operability, and ultimately contributes to MI therapy [13,16–20,25]. In addition, previous studies have demonstrated that MSCs can reduce the apoptosis, improve the maturation, and inhibit the immune rejection of CM [26–28]. Therefore, in this study, we co-cultured human adipose-derived mesenchymal stem cells (hADSCs) with human induced pluripotent stem cell-derived CMs (hiPSC-CMs) on a PLGA fiber scaffold using a one-step seeding process, resulting in the development of composite, highly functional, and well-organized 3D cardiac tissue sheets (as shown in Graphical Abstract).

To the best of our knowledge, this study is the first to generate thick and functional 3D cardiac tissue sheets via composite assembly of hiPSC-CMs and hADSCs. Their organization, contractile properties, and cytokines secretion were assessed *in vitro*. Additionally, their therapeutic effects, including the improvement in cardiac function, reduction in fibrosis, inhibition of remodeling, and promotion of angiogenesis, were evaluated in a rat MI model *in vivo*.

2. Materials and methods

2.1. Construction of poly (lactic-co-glycolic acid) (PLGA) fiber scaffold

To prepare the scaffold, poly (lactic-*co*-glycolic acid) (PLGA) (75/25; molecular weight: 66,000–107000; Sigma-Aldrich, St. Louis, MO, USA) was mixed with hexafluoro-2-propanol (HFIP, Wako Pure Chemical Industries, Tokyo, Japan) in a centrifugal tube (1.2 g:3 mL, w/v). Fibers were synthesized using an automated electrospinning machine (NF-103, MECC, Fukuoka, Japan). The mixed solution was loaded into a 3-mL syringe, to which a needle of 0.6-mm inner diameter was attached, connecting it to the positive electrode of the high-voltage power supply (10 kV). A layer of aluminum foil was attached to the grounded drum, which was rotated at 1000 rpm to collect the PLGA fiber scaffold. The distance between the needle tip and drum was maintained at 15 cm, and spinning was performed for 60 min. Finally, the fiber sheets were transferred to a polydimethylsiloxane (PDMS) frame (1 cm × 1 cm) for subsequent cell seeding. After formation, the fibers were examined using a scanning electron microscope, as previously described [17].

2.2. Preparation and characterization of human-induced pluripotent stem cell-derived cardiomyocytes (hiPSC-CMs)

Human-induced pluripotent stem cells (hiPSCs) (253G1; Riken, Tsukuba, Japan) were cultured in a primate embryonic stem cell medium (ReproCELL, Kanagawa, Japan) supplemented with the basic fibroblast growth factor (bFGF; ReproCELL, Kanagawa, Japan) at 37 °C. Mitomycin Ctreated mouse embryonic fibroblasts (ReproCELL, Kanagawa, Japan) were used as feeder cells. Cardiomyogenic induction was performed in the StemPro 34 medium (Thermo Fisher Scientific, Waltham, MA) containing 2 mM L-glutamine (Thermo Fisher Scientific, Waltham, MA), 50 mg/mL ascorbic acid (Wako, Pure Chemical Industries, Tokyo, Japan), and 400 mM 1-thioglycerol (Sigma-Aldrich, St. Louis, MO), as previously described [18].

To obtain hiPSC-CMs, hiPSCs were dissociated using Accmax (Nacalai Tesque, Kyoto, Japan), and induced in a bioreactor (ABLE Corporation & Biott Co., Tokyo, Japan). Human recombinant bone morphogenetic protein 4 (BMP4), activin A, bFGF, and vascular endothelial growth factor (VEGF) (R&D Systems, Minneapolis, MN), along with the small-molecule compounds IWR-1 and IWP-2 (Sigma-Aldrich, St. Louis, MO) were used for induction as follows: BMP4 from day 0–1; activin A, BMP4, and bFGF from days 1–4; IWR-1 and IWP-2 from days 4–6; and VEGF and bFGF after day 6. Flow cytometry analysis was performed on day 14 using a FACS Canto II (BD, Franklin Lakes, NJ) as previously reported [18].

2.3. Culture of human adipose mesenchymal stromal cells (hADSCs)

Next, hADSCs were obtained from PromoCell (C-12977, PromoCell, Heidelberg, Germany). The hADSCs were cultured and expanded as previously described [25]. Briefly, cryopreserved passage 2 (P2) cells were obtained and cultured in the mesenchymal stem cell (MSC) Xeno-Free culture medium (Takara Bio Inc., Shiga, Japan) at 37 °C in a 5% CO_2 incubator. The culture medium was changed every 2–3 days, and upon reaching 80–90% confluency, the cells were detached using TrypLE Select (Gibco, Waltham, MA, USA) for further expansion. Cells of passages 4–7 were used for all experiments.

2.4. Characterization of human adipose mesenchymal stromal cells (hADSCs)

A flow cytometry (BD FACSCanto II; BD Biosciences, Erembodegem, Belgium) was used for immunophenotyping. hADSCs were harvested after seven passages, dissociated into single cells, washed with phosphate-buffered saline (PBS), and stained with the fluorescence-conjugated antibodies, including the anti-hCD31-PE, anti-hCD34-PE, anti-hCD45-PE, anti-hCD73-PE, anti-hCD90 (Thy1)-PE, anti-hCD105-PE, anti-HLA-G-PE, and anti-HLA-DR-PE antibodies (Table S1). Mouse IgG1 κ isotype was used as a control for cell staining. Antibodies were purchased from BioLegend (San Diego, CA, USA). FlowJo software v10.5.3 (BD, Franklin Lakes, NJ, USA) was used for data analysis.

Differentiation potential of hADSCs into adipogenic, osteogenic, and chondrogenic lineages was evaluated using a differentiation medium (PromoCell, Heidelberg, Germany) for 2, 2, and 3 weeks, respectively. Differentiation of hADSCs was further confirmed via Oil red O, Alizarin red S, and Alcian blue (Sigma-Aldrich) staining, respectively. Samples were examined under a fluorescence microscope (BZ-X800; KEYENCE, Osaka, Japan).

2.5. Cardiomyocyte (CM) tissue sheets and CM + adipose mesenchymal stromal cell (ADSC) tissue sheets formation

To construct CM tissue sheets, hiPSC-CMs were dissociated into single cells with Trypsin-EDTA (GIBCO, Tokyo, Japan) and seeded onto PLGA fiber scaffolds at a density of 5×10^6 cells/cm². Then, 3 μmol/L Rho-kinase (ROCK) inhibitor (FUJIFLIM, Tokyo, Japan) and 10 μg/mL iMatrix-511 (Matrixome, Osaka, Japan) were added during cell seeding. The tissue sheets were cultured in a humidified atmosphere containing 5% CO_2 at 37 °C for 3–5 days before transplantation, and the medium was changed every 2 days.

For CM + ADSC tissue sheet formation, hADSCs from the 2nd passage were seeded in a 100 mm dish (Falcon 353,003, Arizona, USA) after thawing. When the cell confluency reached approximately 70–80%, hADSCs were collected from the dishes and rinsed with PBS. The hiPSC-CMs obtained through the above steps were mixed with hADSCs and seeded onto PLGA fiber scaffolds at a density of 5×10^6 cells/cm² (hiPSC-CMs: hADSCs = 9 : 1). Then, 3 μmol/L ROCK inhibitor (FUJI-FLIM, Tokyo, Japan) and 10 μg/mL iMatrix-511 (Matrixome, Osaka, Japan) were added during cell seeding. The tissue sheets were cultured in a humidified atmosphere containing 5% CO_2 at 37 °C for 3–5 days before transplantation, and the medium was changed every 2 days.

2.6. Western blotting

To isolate total protein, CM + ADSC tissue sheets and CM tissue sheets were dissolved in Radioimmunoprecipitation assay (RIPA) buffer

with protease inhibitor (Thermo Fisher Scientific, Rockford, Illinois, USA), placed on ice for more than 30 min, and centrifuged at $400 \times g$ for 5 min to remove all insoluble matter. Protein concentration was measured using the Bicinchoninic acid (BCA) assay (Thermo Fisher Scientific, Rockford, Illinois, USA). Sodium dodecyl sulfate-polyacrylamide gel electrophoresis was performed by applying 10 μg of protein sample in each lane. After the membrane transfer of the proteins and blocking with EveryBlot Blocking Buffer (Bio-Rad Laboratories, Hercules, CA, USA), the membranes were incubated overnight at 4 °C with the primary antibodies listed in Table S1. Thereafter, they were incubated for 1 h at 25 °C with anti-rabbit or anti-mouse horseradish peroxidase-coupled secondary antibody. Bands were visualized using SuperSignal™ West Atto Ultimate Sensitivity Substrate (Thermo Fisher Scientific) and quantified using a ChemiDoc multiplex fluorescence imaging system (Bio-Rad Laboratories).

2.7. Motion analysis

The contractile properties of CM + ADSC tissue sheets and CM tissue sheets were evaluated using a cell motion imaging system (SI8000; SONY, Tokyo, Japan). The tissues were cultured for 5 days. Videos were recorded at a rate of 150 frames per second, a resolution of 1024×1024 pixels, and a depth of 8 bits. The beating rate, contraction velocity, relaxation velocity, acceleration, contraction deformation distance, and relaxation deformation distance were measured using SI8000C analyzer software (Sony).

2.8. Electrophysiological recording using microelectrode arrays (MEA)

The field potentials of the cardiac tissue were recorded using a MEA data system (USB-ME64-System, Multi-Channel Systems, Germany) with an MC_ Rack (Multi-Channel Systems). The activation map was generated using the local activation time from the single electrodes by calculating the minimum of the raw curve's first-derivative plot. Linear interpolation between the electrodes was used to calculate the isochronal map using MATLAB (MATLAB, MathWorks, USA) [16].

2.9. Seahorse mitochondrial function test

According to the manufacturer's instruction of the seahorse XF Cell Mito Stress Test kit (Agilent, CA, USA), we detected the Oxygen Consumption Rate (OCR) of cells in tissue sheets. Specifically, CM + ADSC tissue sheets and CM tissue sheets were digested into single cells, and after cell counting, 4.0×10^4 cells were seeded in each well of an XFe 96 cell culture plate, and cultured in 37 °C, 5% CO_2 incubator for 24 h. Prior to the experiment, we preheated the machine and hydrated the sensor cartridge. To prepare the detection solution, we added 1 ml of glucose, 1 ml of pyruvate, and 1 ml of ʟ-glutamine to 97 ml of Seahorse XF RPMI medium. This solution was mixed thoroughly and added to the cell plate. The cell plate was then placed in a CO_2-free incubator at 37 °C for 1 h 1.5 μM Oligomycin, 1 μM carbonyl cyanide p-(trifluoromethoxy) phenylhydrazone (FCCP) and 0.5 μM Rotenone + 0.5 μM antimycin A were added to sensor cartridge ports in sequence. Immediately insert the cell culture microplate into the XF96 Extracellular Flux Analyzer (Agilent, CA, USA) and run the Cell Mitochondrial Stress Test. After measuring OCR, cells were lysed and the protein in each well was quantified using the BCA protein quantification kit. All values of OCR parameters calculated were normalized to the quantified protein content. Data were analyzed using Wave software (Agilent, CA, USA).

2.10. In vitro angiogenesis cytokines array

The expression of angiogenesis-related proteins was measured using a RayBio® C-Series Human Angiogenesis Antibody Array C1000 (RayBiotech, Inc., Norcross GA, USA) according to the manufacture's protocols. It is a combination of Human Angiogenesis Antibody Array C1 and C2, which detects 43 human angiogenic factors. Experiments were made using supernatants from two biological samples of CM tissue sheets and CM + ADSC tissue sheets after 24 h of serum-free (Basel DMEM medium only) culture.

Briefly, membranes were incubated with blocking buffer for 30 min at room temperature, after which the supernatant was added and incubated at 4 °C overnight. The membranes were then washed 5 times with washing buffer and incubated with Biotinylated Antibody Cocktail overnight at 4 °C. After 5 times washing, membranes were incubated with HRP-Streptavidin Concentrate for 2 h at room temperature, washed twice, and placed in detection buffer for 2 min. The signals were detected using the ImageQuant Imaging System (ChemiDoc Touch MP, Osaka, Japan, Bio-Rad). Relative cytokine levels were determined by densitometric analysis using the ImageJ software (NIH, Bethesda, MD, USA).

2.11. Enzyme-linked immunosorbent assay (ELISA) assay

The culture supernatants obtained from the CM tissue sheets and CM + ADSC tissue sheets were analyzed using enzyme-linked immunosorbent assay (ELISA), including vascular endothelial growth factor (VEGF, DVE00), hepatocyte growth factor (HGF, DHG00B) and basic fibroblast growth factor (β-FGF, DFB50, R&D Systems, Minneapolis, MN, USA, Quantikine ELISA), and was performed according to the manufacturer's instructions. The absorbance rate was determined using a microplate reader (Powerscan H1, DS Pharma Biomedical, Osaka, Japan) at a wavelength of 450 nm, with the wavelength correction set to 540 nm.

2.12. In vitro tube formation assay

In vitro tube formation assay was performed using Human Umbilical Vein Endothelial Cells (HUVECs) cultured on Matrigel (Corning, Arizona, USA) [29]. In brief, a 96-well plate was coated with Matrigel for 20 min at 37 °C, and the HUVECs were seeded at a density of 1.5×10^4 cells per well. After incubation with supernatant from CM tissue sheets and CM + ADSC tissue sheets for 16 h. Images were taken under a brightfield microscope (OLYMPUS CKX53, Tokyo, Japan). Statistical analysis was performed using the angiogenesis analyzer tool [30] of ImageJ software (NIH, Bethesda, MD, USA).

2.13. Rat myocardial infarction (MI) model and transplantation

All animal procedures were performed in accordance with the guidelines for animal experimentation approved by the Osaka University (01-062-000). Male F344/NJcl-rnu/rnu nude rats (7 weeks old, weight: 175.7 ± 8.7 g; CLEA Japan, Inc., Shizuoka, Japan) were used for all experiments. The rats were observed for one week before MI induction.

The MI model was induced through left anterior descending (LAD) coronary artery ligation under mechanical ventilation as previous described [31]. Briefly, rats were anesthetized by 1.5% isoflurane inhalation (Mylan Inc., Canonsburg, PA, USA), incubated, and placed on respirator during surgery to maintain ventilation. Thoracotomy was performed between the fourth and fifth intercostal spaces, and MI was induced by permanently ligating the LAD coronary artery with a non-absorbable 6-0 polypropylene suture (Ethicon, Johnson & Johnson, USA). Two weeks after left coronary artery ligation (week 0), transthoracic echocardiography was performed to validate the extent of MI. And the rats with left ventricular (LV) ejection fraction (EF) > 55% were excluded.

These model rats were randomly divided into four groups: (1) thoracotomy without LAD ligation (Sham group), (2) MI model without treatment (MI group) (3) transplantation of CM tissue sheets (CM group), (4) transplantation of CM + ADSC tissue sheets (CM + ADSC group). In the MI group, no intervention was performed except for thoracotomy. For transplantation, the PDMS frame of PLGA fiber

scaffold was cut and removed, and the pericardium was peeled back to identify the infarcted area. The tissue sheets were placed directly onto the infarcted area of heart between the visceral and parietal pericardium. Four weeks after transplantation, the rats were sacrificed through an anesthetic overdose and the hearts were harvested for further analysis.

2.14. Echocardiography

Echocardiographic imaging was performed as previously described. Briefly, rats were maintained under 1.5% isoflurane anesthesia, and kept warm on a heated platform. Transthoracic echocardiographic examinations were then performed on the rats under inhaled isoflurane anesthesia by a blinded technician. Two-dimensional (2D) bright mode (B-mode) and motion mode (M-mode) were obtained from a parasternal long-axis view with a micro-ultrasound system (Vivid i, GE Healthcare, WI, USA). The left ventricle internal diameter at end-systole (LVIDs) and left ventricle internal diameter at end-diastole (LVIDd) were determined from M-mode images, using averaged measurements from four cardiac cycles, in accordance with the American Society of Echocardiography guidelines. The left ventricle end-systolic volume (LVESV) and end-diastolic volume (LVEDV) were then calculated using the Teichholz method:

$$LVESV = \frac{7 \times LVIDs^3}{2.4 + LVIDs}$$

$$LVEDV = \frac{7 \times LVIDd^3}{2.4 + LVIDd}$$

Other parameters such as ejection fraction, fractional shortening (FS) was calculated:

$$LVEF = 100 \times \frac{LVEDV - LVESV}{LVEDV}$$

$$LVFS = 100 \times \frac{LVIDd - LVIDs}{LVIDd}$$

2.15. Immunofluorescence and histological analysis

The CM tissue sheets and CM + ADSC tissue sheets were fixed in 4% paraformaldehyde for 0.5 h and cryosections were prepared for immunohistology. The cryosections were incubated with primary antibodies (for detailed information on antibodies, refer to Table S1) for overnight at 4 °C, followed by washing with PBS and incubation with respective secondary antibodies at 37 °C for 1 h. After counterstaining with 2-(4-amidinophenyl)-1H-indole-6-carboxamidine (DAPI) or Hoechst 33,342, the sections were observed under a fluorescence microscope (BZ-X800; KEYENCE, Osaka, Japan) and a confocal microscope (Nikon A1, Nikon, New York, NY, USA).

After four weeks of transplantation, the rats were euthanized for heart tissue harvesting through echocardiography. Following this, the samples were fixed in formalin, transferred to ethanol, and embedded in paraffin. Serial sections, 5-μm in thickness, were prepared to examine normal tissue architecture using hematoxylin and eosin (H&E) staining. For immunohistology of heart tissue sections, dewaxed paraffin sections were washed in PBS, and antigen retrieval was performed in Target Retrieval Solution (pH = 6; DAKO Japan, Inc, Tokyo, Japan) at 121 °C for 10 min. The sections were stained as described above.

2.16. Terminal deoxynucleotidyl transferase dUTP nick end labeling (TUNEL) staining

Cryosections prepared above were also used for TUNEL staining using the Click-iT TUNEL kit (C10619 Invitrogen, ThermoFisher Scientific, Waltham, MA, USA) following the manufacturer's instructions. And the sections were observed under a confocal microscope (Nikon A1,

Nikon, New York, NY, USA). The percentage of apoptotic nuclei was calculated by dividing the total number of TUNEL-stained nuclei by the total number of Hoechst-positive nuclei using ImageJ software (NIH, Bethesda, MD, USA).

2.17. Infarct size

The infarct size was measured using Masson's trichrome staining, and the fibrosis area was evaluated using picrosirius red staining as described previously [13]. Digital images of stained sections were captured via light microscope (BZ-X800; KEYENCE, Osaka, Japan) and analyzed with ImageJ software (NIH, Bethesda, MD, USA). Infarct size was calculated as follows:

$$\frac{epicardial\ infarct\ ratio + endocardial\ infarct\ ratio}{2} \times 100$$

The epicardial infarction ratio was calculated by dividing the epicardial infarction length by the epicardial circumference, and the endocardial infarction ratio was calculated in a similar manner. The percentage of fibrotic area was calculated as the average ratio of the fibrotic area to the total LV area:

$$percentage\ of\ fibrotic\ area = \frac{fibrotic\ area}{total\ LV\ area} \times 100$$

2.18. Vascular density

To quantify the density of neovessels and arterioles in the graft and the MI border zone of host, von Willebrand Factor (vWF) and alpha-smooth muscle actin (α-SMA) were used to stain the endothelial cells and vascular smooth muscle cells, respectively, while cell nuclei were counterstained blue for DAPI. The neovessels were represented by orange staining, and orange/green double staining represented arterioles, as previously reported [25]. Images were captured using a confocal microscope (Nikon A1, Nikon, New York, NY, USA) and analyzed with ImageJ software (NIH, Bethesda, MD, USA).

2.19. Statistical analysis

All quantitative data are presented as mean ± standard deviation (SD) and were analyzed using GraphPad Prism 9.5.0 (GraphPad Software, USA). The difference in normal variates was tested using Student's *t*-test within the two groups. One-way analysis of variance (ANOVA) followed by Tukey's post-hoc test (variance homogeneity) was used for comparisons among three or more groups. Statistical significance was defined as a *p*-value <0.05, (significance was set at $*p < 0.05$, $**p < 0.01$, and $***p < 0.001$).

3. Results

3.1. Characterization of human-induced pluripotent stem cell-derived cardiomyocytes (hiPSC-CMs)

Human-induced pluripotent stem cells (hiPSCs) were differentiated into hiPSC-CMs as previously reported (Fig. 1A), and subsequent assessments confirmed the expression of the appropriate lineage markers. Flow cytometry analysis was performed on day 14, and the percentage of cardiac troponin T (cTnT)-positive cells was 90.2 ± 1.6 % (Fig. 1B). Immunofluorescence staining revealed that the hiPSC-CMs expressed α-actinin and cTnT (Fig. 1C and D), indicating a well-arranged and clear sarcomeric structure native to cardiomyocytes (CMs). Furthermore, immunofluorescence staining for N-Cadherin and connexin 43 (Cx43) revealed cell-cell communications and gap junctions between hiPSC-CMs (Fig. 1C and D). These results demonstrated the successful differentiation of hiPSCs into high-purity functional CMs.
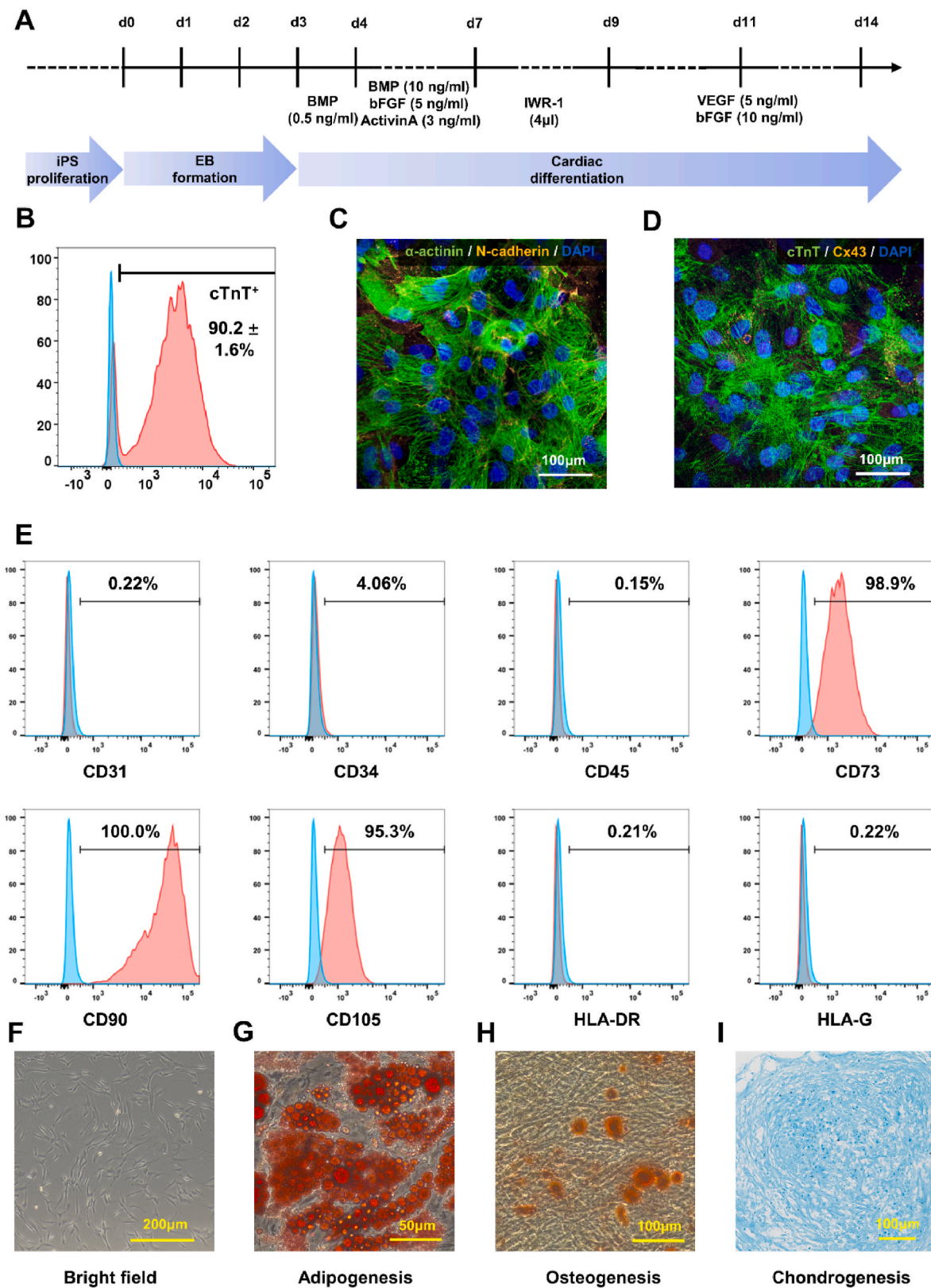
Fig. 1. Characterization of human adipose-derived stem cells (hADSCs) and human induced pluripotent stem cell-derived cardiomyocyte (hiPSC-CMs). (A) Schematic diagram of cardiomyocytes induction from hiPSCs. (B) Representative induction rate of hiPSC-CMs (cTnT). (C) Immunostaining of α-actinin (green) and N-cadherin (orange) in hiPSC-CMs. Nuclei were counterstained with DAPI (blue). Scale bar = 100 μm. (D) Immunostaining of cardiac troponin T (cTnT) (green) and connexin 43 (CX43) (orange) in hiPSC-CMs. Nuclei were counterstained with DAPI (blue). Scale bar = 100 μm. (E) Flow cytometry analysis of hADSCs surface markers CD31, CD34, CD45, CD73, CD90, CD105, HLA-DR, and HLA-G. (F) Bright field microscopic images showing the spindle-like morphology of hADSCs. Scale bar = 200 μm. (F–H) Differentiation potential of hADSCs demonstrated by detection of adipocytes (using Oil Red O staining), osteoblasts (using Alizarin Red staining), and chondrocytes (using Alcian Blue staining). Scale bars = 50 μm, 100 μm, and 100 μm, respectively.

3.2. Characterization of human adipose mesenchymal stromal cells (hADSCs)

To confirm the characterization of hADSCs, flow cytometry-based analysis was performed to determine the expression levels of specific surface markers for mesenchymal stem cells (MSCs) at passage 7. Our data revealed that hADSCs were highly positive for CD73, CD90, and CD105, while significantly negative for CD31, CD34, CD45, HLA-G, and HLA-DR (Fig. 1E). In addition, bright-field microscopy revealed that the cells exhibited a typical spindle-like morphology (Fig. 1F). *In vitro* differentiation assays were performed after the 4th passage to determine whether the hADSCs retained their differentiation potential. The plasticity of hADSCs was confirmed via adipogenic, osteogenic, and chondrogenic differentiation using Oil red O (adipogenic marker) (Fig. 1C), Alizarin S red (osteogenic marker) (Fig. 1D), and Alcian blue (chondrogenic markers) (Fig. 1E) staining, respectively. The expression profiles of these surface markers and their differentiation abilities were consistent with the properties of MSCs.

3.3. Development and evaluation of CM and CM + ADSC tissue sheets

The Poly (lactic-*co*-glycolic acid) (PLGA) fiber scaffold was utilized as a culture substrate to facilitate tissue formation by hADSCs and hiPSC-CMs. Based on the Hematoxylin and Eosin (HE) staining results (Fig. 2A), CM tissue sheets and CM + ADSC tissue sheets showed a thickness of 185.52 ± 16.02 μm and 231.00 ± 15.14 μm (Fig. 2E), respectively. Furthermore, the terminal deoxynucleotidyl transferase dUTP nick end labeling (TUNEL) staining was used to evaluate the viability of cells within the tissues (Fig. 2B), the apoptotic rate of CM + ADSC tissue sheets was lower than that of CM tissue sheets (Fig. 2F). In
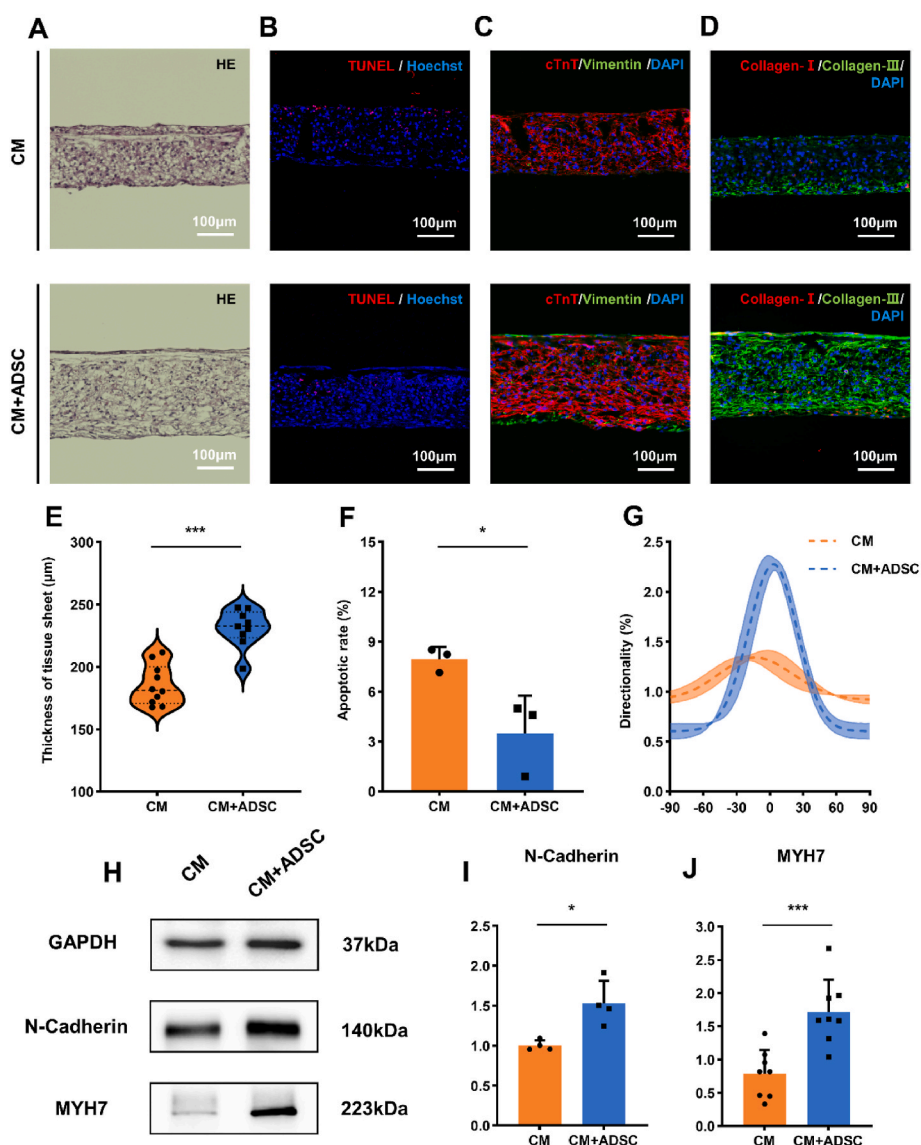

Fig. 2. Construction and evaluation of CM + ADSC tissue sheets. (A) Hematoxylin and eosin (HE) staining of CM and CM + ADSC tissue sheet (side view). Scale bar = 100 μm. (B) TUNEL staining of CM and CM + ADSC tissue sheet. Nuclei were counterstained with Hoechst (blue). Scale bar = 100 μm. (C) Immunohistochemical staining of vimentin (green) and cTnT (red) expression in the CM and CM + ADSC tissue sheet. Nuclei were counterstained with DAPI (blue). Scale bar = 100 μm. (D) Immunohistochemical staining of collagen I (green) and collagen III (red) expression in the CM and CM + ADSC tissue sheet. Nuclei were counterstained with DAPI (blue). Scale bar = 100 μm. (E) Quantitative analysis of thickness of CM and CM + ADSC tissue sheet. (F) Quantitative analysis of apoptotic rate in CM and CM + ADSC tissue sheet. (G) Fourier component analysis of iPSC-CMs in CM and CM + ADSC tissue sheet. (H) Representative western blots (WB) of MYH7, N-Cadherin, and GAPDH from CM and CM + ADSC tissue sheet. (I–J) Quantification of protein expression from WB by densitometry, normalized to GAPDH, in the CM and CM + ADSC group, *n* represented independent experiment samples. Results are presented as mean $\pm$ SD. Statistical significance was determined using Student's *t*-test. *$p < 0.05$, ***$p < 0.001$.

addition, immunostaining revealed a well organization of CM + ADSC tissue sheets and CM tissue sheets (Fig. 2C and Fig. S1A), however, the CM + ADSC tissue sheets exhibited improved alignment of hiPSC-CMs within the tissues than that of CM tissue sheets (Fig. 2G). As shown in Fig. 2D and Fig. S1B and a more abundant expression of extracellular matrix (ECM) was observed in CM + ADSC tissue sheets in comparison to the CM tissue sheets. Moreover, we also found that the proliferation rate in CM tissue sheet and CM + ADSC tissue sheet remained at relatively low levels (Fig. S2). In CM + ADSC tissue sheets, N-Cadherin and Myosin Heavy Chain 7 (MYH7) showed markedly higher expression than those of the CM tissue sheets (Fig. 2H–J). In conclusion, the CM + ADSC tissue sheets exhibited superior tissue organization compared to CM tissue sheets.

3.4. Contractile and respiration properties of CM and CM + ADSC tissue sheets

To evaluated the contractility of CM + ADSC tissue sheets, we performed motion analysis using a high-speed camera-based motion analysis system as described above. Fig. 3A depicted the high-velocity area as red, middle-velocity area as green, and low-velocity area as blue. Contraction velocity, relaxation velocity, and acceleration were significantly higher in CM + ADSC tissue sheets than that in CM tissue sheets (Fig. 3B–D). Moreover, the contraction deformation distance and relaxation deformation distance were remarkably longer in CM + ADSC tissue sheets than that in CM tissue sheets (Fig. 3E and F). However, the beating rate of CM + ADSC tissue sheets is lower than that of CM tissue
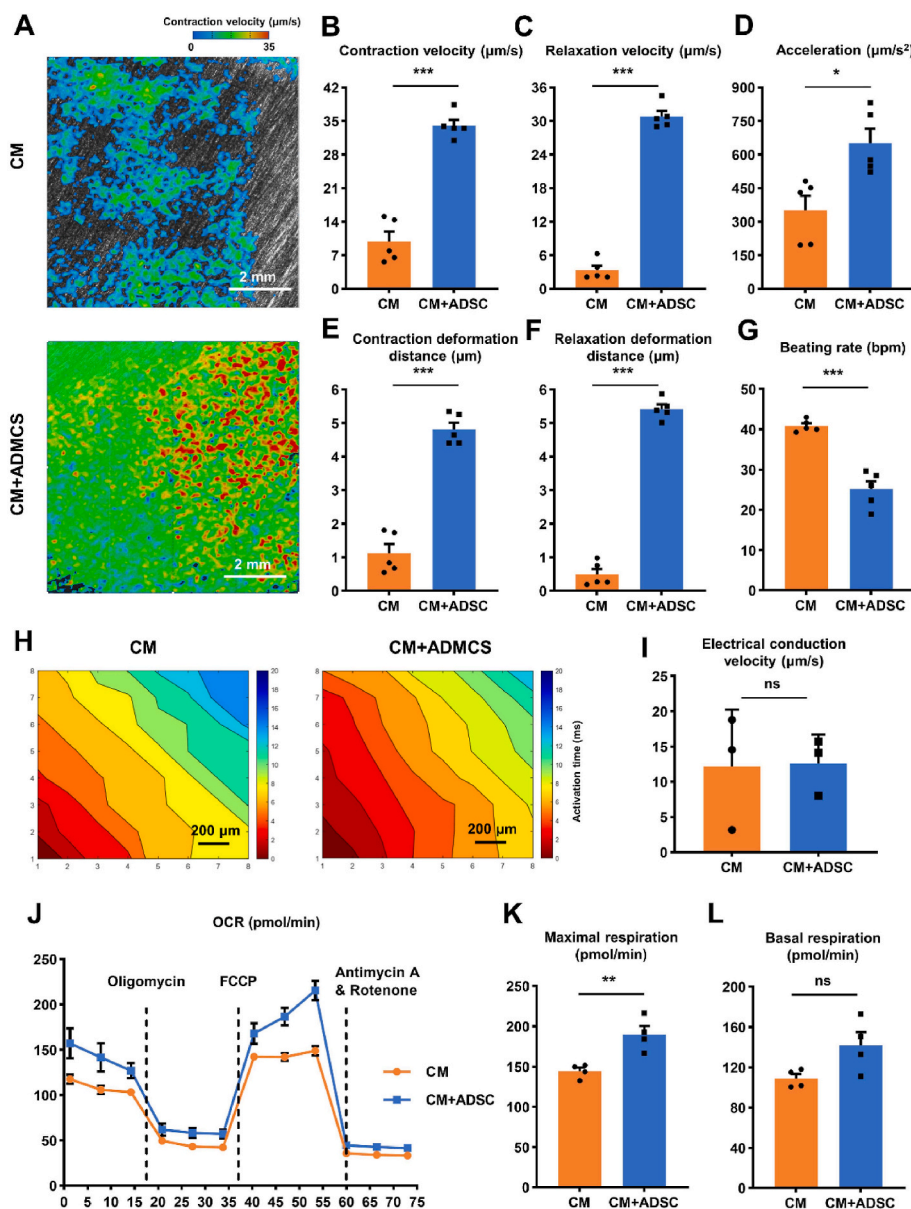
Fig. 3. Contractile and respiration properties of CM and CM + ADSC tissue sheets. (A) Representative velocity image of the cardiac tissue on CM and CM + ADSC tissue sheet using a motion analysis system. Red, green, and blue color represent high, middle and low velocities, respectively. Scale bar = 2 mm. (B–G) Motion analysis parameters of CM and CM + ADSC tissue sheet: contraction velocity (B), relaxation velocity (C), acceleration (D), contraction deformation distance (E), and relaxation deformation distance (F), and beating rate (G). (H) Map of conduction velocity of cardiac tissue on CM and CM + ADSC tissue sheet using a microelectrode arrays (MEA) data system. Scale bar = 200 μm. (I) Quantitative analysis of conduction velocity of cardiac tissue on CM and CM + ADSC tissue sheet. (J) Representative traces showing the OCR of cells in CM and CM + ADSC tissue sheet following sequential addition of oligomycin, carbonyl cyanide p-(trifluoromethoxy) phenylhydrazone (FCCP), and rotenone/antimycin A. (K–L) Quantitative analysis of maximal respiration (K) and basal respiration (L). Results are presented as mean ± SD. Statistical significance was determined using Student's *t*-test. *$p < 0.05$, **$p < 0.01$, and ***$p < 0.001$, ns means no statistical significance.

sheets (Fig. 3G). Therefore, the CM + ADSC tissue sheets had improved contractile properties compared to the CM tissue sheets.

Furthermore, electrophysiological data recorded using Microelectrode Arrays (MEA) indicated there is no significant differences in electrical conduction velocity between CM + ADSC tissue sheets and CM tissue sheets (Fig. 3H and I). To characterize mitochondrial function, we detected tissue sheets using the seahorse XF assay. Fig. 3J showed representative traces of cells in CM + ADSC group and CM group. The CM + ADSC group had significantly higher maximal respiration than the CM group (Fig. 3L), whereas the basal respiration in CM + ADSC group was similarly to that in CM group (Fig. 3K). Therefore, we concluded that CM + ADSC tissue sheets exhibited stronger mitochondrial function.

### 3.5. Cytokines secretion and angiogenesis function of CM and CM + ADSC tissue sheets

In order to examine the cytokines secretion ability of the CM and CM + ADSC tissue sheets, a cytokines secretion assay using the Human Cytokine Antibody Array C5 was performed at first. The cytokines released from the CM tissue sheets and CM + ADSC tissue sheets was shown in Fig. 4A. The results revealed that the abundance of C-X-C motif chemokine 5 (CXCL5), GRO, CXCL1, Interleukin 6 (IL-6), IL-8, Chemokine (C–C motif) ligand 8 (CCL8), CCL7, CCL5, stromal cell-derived factor 1 (SDF-1), Angiogenin, Vascular endothelial growth factor A (VEGF-A), Hepatocyte growth factor (HGF), Macrophage Inflammatory

Protein-3 (MIP-3α), secreted phosphoprotein 1 (SPP-1), and Tumor Necrosis Factor Receptor Superfamily Member (TNFRSF11) were obviously higher in the culture supernatant of CM + ADSC tissue sheets than in that of CM tissue sheets (Fig. 4B). To further investigated the secretion of VEGF, HGF, and basic fibroblast growth factor (bFGF), which were related to blood vessels formation and fibrosis reduction, we performed quantitative analysis by enzyme-linked immunosorbent assay (ELISA). As shown in Fig. 4C–E, we can know that the concentration of VEGF, HGF, and bFGF in the supernatant of CM + ADSC tissue sheets was significantly higher than those in CM tissue sheets.

To further investigated the angiogenesis function of CM + ADSC tissue sheets, an angiogenic cytokines secretion assay was performed using Human Angiogenesis Antibody Array C1000. Fig. 5A and B depicted that the abundance of Angiogenin, GRO, IL-6, IL-8, CCL5, Tissue Inhibitor of Metalloproteinase (TIMP)-1, TIMP-2, VEGF-A, Angiopoietin 1 (ANGPT1), ANGPT2, CCL7, Matrix metalloproteinase-9 (MMP-9), and urokinase-type plasminogen activator receptor (uPAR) were significantly higher in the culture supernatant of CM + ADSC tissue sheets than in that of CM tissue sheets (Fig. 5C). In addition, the results of *in vitro* tube formation assay demonstrated that supernatant of CM + ADSC tissue sheets remarkably enhanced angiogenesis in HUVEC cells compared to that of CM tissue sheets (Fig. 5D). The image analysis results indicated that the mesh count and branch count of CM + ADSC group was notably higher than those of CM group (Fig. 5E and F), and the total length of tubes in CM + ADSC group was markedly longer than that in CM group (Fig. 5G).
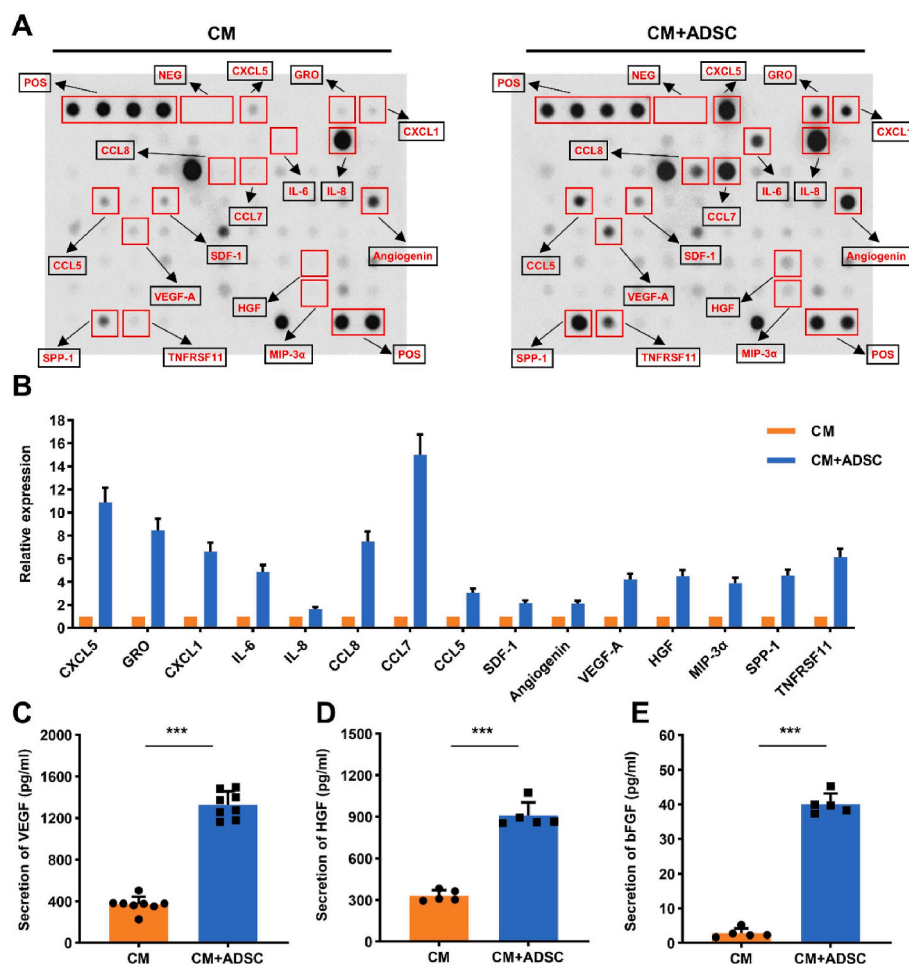
Fig. 4. Comparison of cytokine secretion between CM and CM + ADSC tissue sheet. (A) Representative images of cytokine antibody arrays from the supernatant of CM and CM + ADSC tissue sheet. Highlighted rectangles indicate the elevated cytokines; POS means positive control spots; NEG means negative control spots. (B) Relative secretion of cytokines by CM and CM + ADSC tissue sheet. (C–E) Comparison of VEGF, HGF, and bFGF secretion in the supernatant of CM and CM + ADSC tissue sheet. Results are presented as mean ± SD. Statistical significance was determined using Student's *t*-test. ***$p < 0.001$.
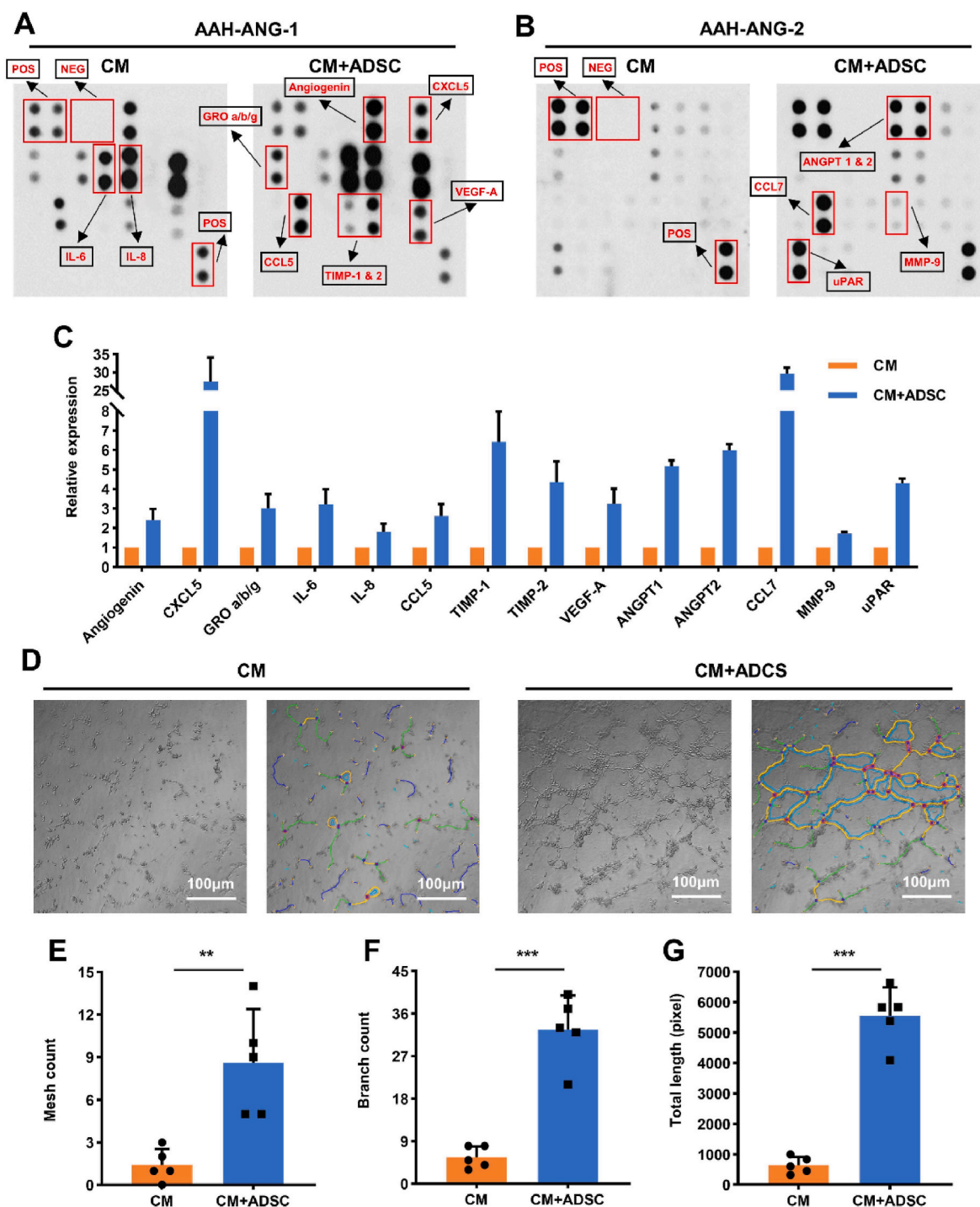
Fig. 5. Evaluation of angiogenesis function of CM and CM + ADSC tissue sheets. (A–B) Representative images of angiogenesis related cytokine antibody arrays from the supernatant of CM and CM + ADSC tissue sheet. Highlighted rectangles indicate the elevated cytokines; POS means positive control spots; NEG means negative control spots. (C) Relative secretion of angiogenesis related cytokines by CM and CM + ADSC tissue sheet. (D) Representative image of tube formation assay on Matrigel in HUVEC cells using supernatant from CM and CM + ADSC tissue sheet. Scale bar = 100 μm. (E–G) Quantitative analysis of angiogenesis related parameters in tube formation assay: mesh count (E), branch count (F), total length (G). Results are presented as mean ± SD. Statistical significance was determined using Student's *t*-test. *$p < 0.01$, ***$p < 0.001$.

From the findings above, we concluded that the CM + ADSC tissue sheets exhibit an enhanced cytokines secretion function, particularly in the paracrine factors related to angiogenesis.
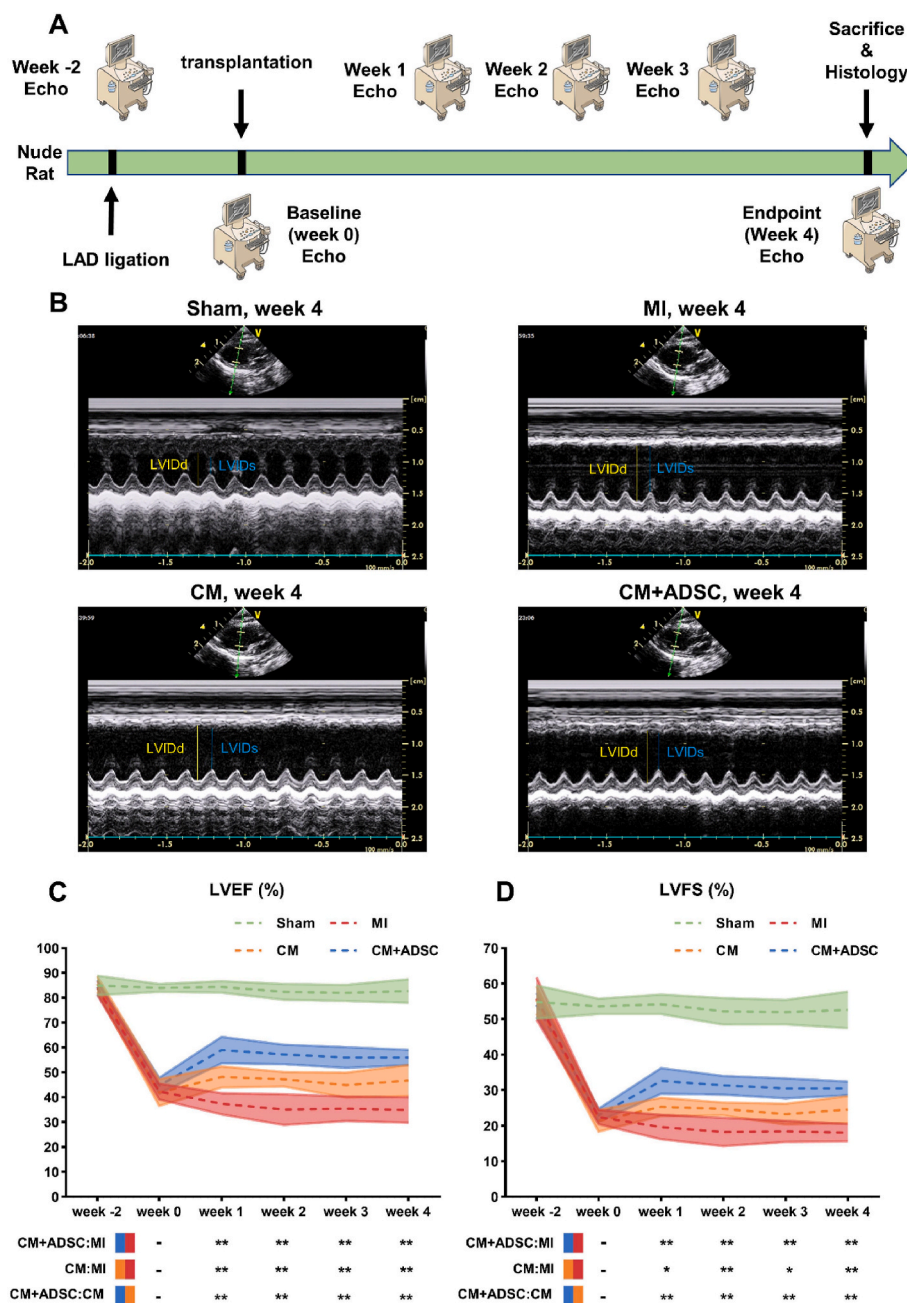
3.6. Transplantation of CM + ADSC tissue sheets improved cardiac function

To further investigate the therapeutic efficacy of the CM + ADSC tissue sheets, CM and CM + ADSC tissue sheets were transplanted into rat models. To evaluate the cardiac function of rats, echocardiography was performed before (week −2) and 2 weeks after (week 0) left anterior

descending artery (LAD) ligation and at 1, 2, 3, and 4 weeks after transplantation of the CM and CM + ADSC tissue sheets (Fig. 6A and B). The initial left ventricular ejection fraction (LVEF), left ventricular fractional shortening (LVFS) showed no significant differences among the Sham group (Fig. 6C and D, green), MI group (Fig. 6C and D, red), CM group (Fig. 6C and D, orange), and CM + ADSC group (Fig. 6C and D, blue). The noticeable decrease in LVEF and LVFS in all ischemic model groups (MI group, CM group, and CM + ADSC group) at week 0 confirmed the success of LAD ligation. In addition, at week 0, no significant differences were observed in LVEF and LVFS among the ischemic model groups (Fig. 6C and D).

As shown in Fig. 6C, the LVEF values were significantly higher in the

CM + ADSC group than those in the CM group and MI group at week 1 (CM + ADSC 58.97 ± 5.37 % versus CM 48.16 ± 4.28 % [$p = 0.0015$] versus MI 37.39 ± 4.24 % [$p = 0.0010$]), week 2 (CM + ADSC 57.23 ± 3.96 % versus CM 47.22 ± 2.97 % [$p = 0.0019$] versus MI 35.08 ± 6.17 % [$p = 0.0010$]), week 3 (CM + ADSC 55.96 ± 4.19 % versus CM 44.89 ± 5.03 % [$p = 0.0010$] versus MI 35.37 ± 4.92 % [$p = 0.0010$]), and week 4 (CM + ADSC 55.97 ± 3.06 % versus CM 46.68 ± 6.32 % [$p = 0.0064$] versus MI 34.89 ± 5.15 % [$p = 0.0010$]) after transplantation. Similarly, the LVFS values were significantly higher in the CM + ADSC group than those in the CM and MI groups at 1, 2, 3, and 4 weeks after transplantation, and the trend in the LVFS values was consistent with that of the LVEF values (Fig. 6D).cc.

Fig. 6. CM + ADSC tissue sheets transplantation improves cardiac function. (A) The study protocol of the animal experiment and the evaluation of cardiac function and histological analysis. (B) Representative M-mode echocardiography images of the Sham group, MI group, CM group, and CM + ADSC group at week 4. (C–D) LVEF (C) and LVFS (D) assessed by echocardiography in the Sham group, MI group, CM group, and CM + ADSC group before MI, before transplantation (week 0), and 1, 2, 3, 4 weeks post-transplantation, respectively (Sham group, n = 4; MI group, n = 6; CM group, n = 6; CM + ADSC group, n = 8). The results are presented as mean ± SD. Significance was determined using one-way ANOVA followed by Tukey's post hoc test. *$p < 0.05$, **$p < 0.01$.

These findings demonstrated that the CM + ADSC tissue sheets exhibit a significant therapeutic effect on recovery of cardiac function after myocardial infarction compared with the CM tissue sheets.

3.7. Transplantation of CM + ADSC tissue sheets inhibited hypertrophy and promoted graft engraftment of hiPSC-CMs

To assess cardiac hypertrophy, we performed HE staining and wheat germ agglutinin (WGA) staining of heart samples from the four groups obtained 4 weeks post-transplantation (Fig. 7A and B). In the border zone, the average diameter (short-axis traversing the cell nuclei) of CMs in the MI group was significantly longer than that in Sham group, however, the average diameter of CMs in CM + ADSC group and CM group were remarkably shorter than that in the MI group, indicating that the transplantation of tissue sheets inhibited CM hypertrophy (Fig. 7B and C).

Transplantation tissue engraftment was evaluated via immunofluorescent staining (Fig. 7D and E) to confirm the presence of graft retention and the angiogenesis status. To analyze the graft retention, the hcTnT was used to label the engraftment hiPSC-CMs, cells within the graft were marked, whereas the CMs of host showed no reactivity (Fig. 7D). The CM + ADSC group showed a higher visible graft retention rate compared with CM group (CM + ADSC: 4 out of 8 rats; CM: 1 out of 6 rats) (Fig. 7F). In addition, as shown in Fig. 7D, we can also observe that hiPSC-CMs within the graft in the CM + ADSC group had a higher density and better alignment (Fig. 7D). To investigate the angiogenesis status within graft, von Willebrand factor (vWF) and α-smooth muscle actin (α-SMA) were used to stain the endothelial cells and vascular smooth muscle cells, respectively. There are more vWF-positive cells and α-SMA-positive cells in the grafts of CM + ADSC group than that of CM group, indicates enhanced angiogenesis in CM + ADSC group (Fig. 7E).

Based on the above findings, the application of CM + ADSC tissue sheets transplantation inhibited cardiac hypertrophy, enhanced the graft retention and the internal angiogenesis of the graft.

3.8. Transplantation of CM + ADSC tissue sheets decreased cardiac fibrosis and promoted angiogenesis in host

To investigate the mechanisms underlying the improvements in cardiac function, we examined the extent of cardiac fibrosis through Masson's staining and Sirius Red staining. The CM + ADSC group showed significantly decreased fibrotic area compared to the CM group, while the fibrotic area of CM group was remarkably decreased than that of MI group at 4 weeks post-transplantation (Fig. 8A and B). Similar as the trend of fibrotic area results, the CM + ADSC group exhibited reduced infarct size than those in CM group and MI group 4 weeks after transplantation (Fig. 8C and D).

Furthermore, the formation of new blood vessels in MI border zone of host was evaluated by using immunofluorescence staining. Fig. S3 showed the status of blood vessels without MI in sham group. The application of CM + ADSC tissue sheets strongly augmented the preservation or formation of neovessels, as shown by immunostaining for vWF, and the arteriolar response, as shown by co-immunostaining for vWF & α-SMA (Fig. 8E and F). As shown in Fig. 8E-H, the density of neovessels was remarkably higher in the CM + ADSC group than that in CM group and MI group. Moreover, the arteriolar density was also significantly higher in the CM + ADSC group than CM group and MI group. However, there is no significant differences in both neovessels and arteriolar densities between CM group and MI group.

In summary, these findings suggested that CM + ADSC tissue sheets exhibited a significant effect in preventing cardiac fibrosis and promoting angiogenesis in the ischemic heart compared to CM tissue sheets.

4. Discussion

In this study, we developed a composite, highly functional, and well-organized 3D cardiac tissue sheet by co-culturing hiPSC-CMs with hADSCs on a PLGA fiber scaffold. We found that the CM + ADSC tissue sheets exhibited abundant ECM deposition and potent cytokine secretion, especially of factors related to angiogenesis, such as angiogenin, ANGPT1 and 2, and VEGF-A. Moreover, the alignment, protein expression, and function of hiPSC-CMs in the tissue sheets were also significantly improved. This study is the first to report the efficacy and therapeutic potential of hiPSC-CM/hADSC 3D composite tissue sheets in an MI rat model. The CM + ADSC tissue sheets were transplanted onto the epicardial surface of rat hearts. Echocardiographic data indicated a significant improvement in cardiac function following cell sheet transplantation. Furthermore, the histological results of heart samples showed a decrease in cardiac hypertrophy and fibrotic area/infarct size, and an increase in engraftment retention and neovascular density (Fig. 9).

Numerous studies have highlighted the ability of iPSC-CMs to engraft, establish a functional myocardium, and further improve the cardiac function in diverse animal models of MI [22,32]. PLGA is a biodegradable and biocompatible copolymer that has been used in FDA-approved therapeutic devices including several in our previous studies [16,18,19,24,25,33]. Our previous studies have demonstrated that constructing and organizing hiPSC-CMs into tissue sheets using PLGA fiber scaffold *in vitro* could enhance their therapeutic capabilities after transplantation [17,19,34]. Additionally, we attempted to enhance the function of tissue sheets and their therapeutic effects in *vivo* through several methods, such as physical stimulation [20], utilization of pharmaceutical agents [18], and stacking multiple fibers [16]. However, despite improvements in engraft retention achieved through the above approaches, there are still remaining issues in therapeutic efficacy because of the limited paracrine functions of exogenous hiPSC-CMs [16, 18,20,35]. MSCs are considered a promising approach for repairing damaged myocardium after MI, improving LV function and remodeling, and enhancing neovascularization via various paracrine cytokines [36]. In our previous studies, we demonstrated that the construction of solid and functional tissue sheets using PLGA fiber scaffolds and MSCs exhibited enhanced therapeutic effects compared to the single-cell suspensions [25].

This study was designed to investigate whether hADSCs can enhance tissue organization and function *in vitro*, augment the retention of transplanted tissue sheets and whether the composite 3D cardiac tissue sheets therapy can improve the heart function recovery. In our study, the co-cultured hiPSC-CMs and hADSCs constructed a composite 3D cardiac tissue with superior thickness, viability, and alignment of the tissue sheet compared with the hiPSC-CM only counterpart (Fig. 2). Furthermore, the CM + ADSC tissue sheets exhibited enhanced contractile ability and mitochondrial function than that of CM tissue sheets (Fig. 3). These enhancements may be related to the abundant expression of ECM and paracrine cytokines secretion by hADSCs [26,37,38]. The paracrine effects are considered as the primary mechanism underlying the ability of transplanted cells to induce cardiac repair [39,40]. According to our study, the CM + ADSC tissue sheet showed a remarkably improvement in paracrine cytokines secretion than that of CM tissue sheet, especially in angiogenesis-related cytokines (Figs. 4 and 5). Importantly, these angiogenesis-related cytokines not only contributed to the vascular formation of rat heart but also simultaneously affect the tissue sheet itself, which could be confirmed by the evaluation of neovessels (vWF$^+$) and arterioles (vWF$^+$ & α-SMA$^+$), and the angiogenesis results in tissue sheets eventually improved the graft retention after 4 weeks transplantation (Fig. 7).

Here, our fundamental and final aim was to improve the cardiac function and alleviate the damage caused by severe MI. We used the LV long-axis view method to evaluate the cardiac function and reduce the errors caused by the different selections of the short-axis, and thereby enhance the accuracy and reproducibility of LVEF and LVFS (Fig. 6). Compared with the CM group, CM + ADSC group showed more significant increase in LVEF and LVFS, which may be related to the better
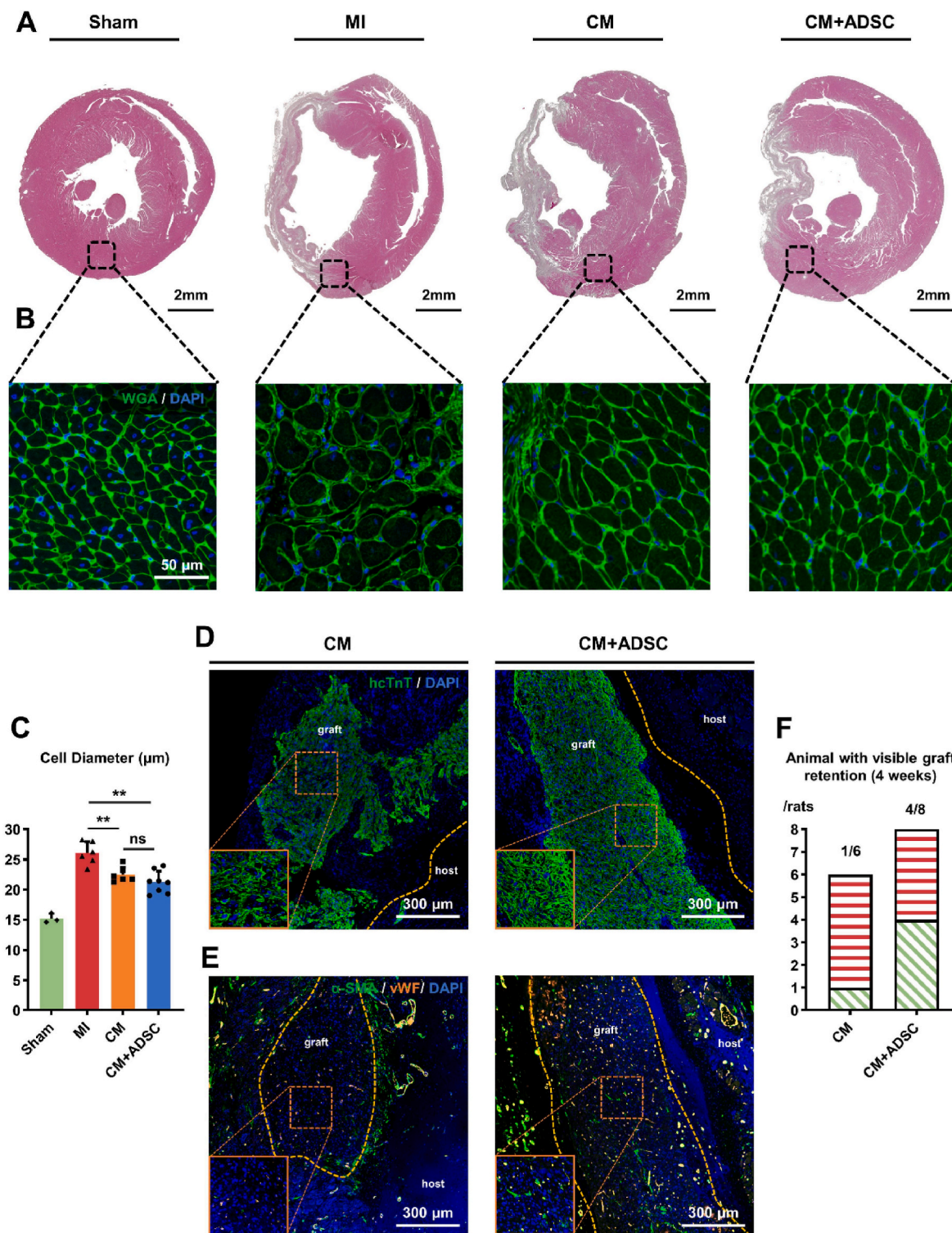
Fig. 7. CM + ADSC tissue sheets transplantation inhibits hypertrophy and promotes graft engraftment of hiPSC-CMs. (A) Hematoxylin and eosin (H&E) staining of Sham group, MI group, CM group, and CM + ADSC group at the papillary muscle level, respectively. Scale bar = 2 mm. (B) Wheat germ agglutinin (WGA) staining of the myocardium in the border zone with DAPI counterstaining. Scale bar = 50 μm. (C) Quantitative analysis of MI border zone cardiomyocyte cell diameter (short-axis) Sham group, MI group, CM group, and CM + ADSC group, respectively. (D) Immunohistochemical staining of hcTnT (green) expression in the CM and CM + ADSC group at 4 weeks post-transplantation. Nuclei were counterstained with DAPI (blue). Scale bar = 300 μm. (E) Immunohistochemical staining of α-SMA (green) and vWF (orange) expression in the CM and CM + ADSC group at 4 weeks post-transplantation. Nuclei were counterstained with DAPI (blue). Scale bar = 300 μm. (F) Statistic showing the animal with visible graft retention in CM and CM + ADSC group. The results are presented as mean ± SD. Significance was determined using one-way ANOVA followed by Tukey's post hoc test. $**p < 0.01$, ns means no statistical significance.
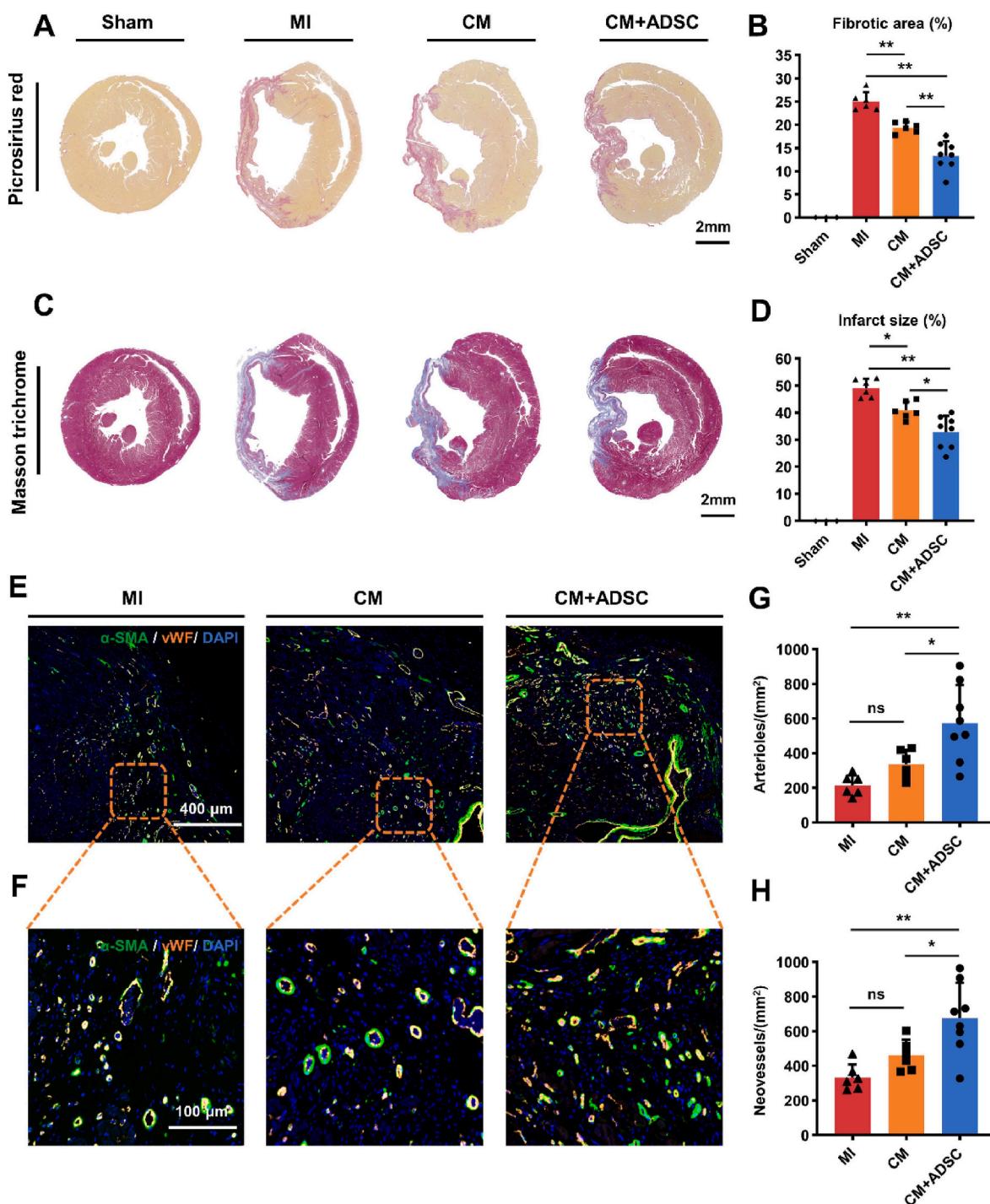
Fig. 8. Assessment of cardiac fibrosis and angiogenesis at 4 weeks post-transplantation (A) Picrosirius red staining images of Sham group, MI group, CM group, and CM + ADSC group are displayed, respectively. Scale bar = 2 mm. (B) Quantitative analysis of fibrotic area in Sham group, MI group, CM group, and CM + ADSC group at 4 weeks post-transplantation. (C) Masson trichrome staining images of Sham group, MI group, CM group, and CM + ADSC group are presented, respectively. Scale bar = 2 mm. (D) Quantitative analysis of infarct size in Sham group, MI group, CM group, and CM + ADSC group at 4 weeks post-transplantation. (E–F) Immunostaining of vWF (orange), α-SMA (green), and nuclei (blue) in the ischemic heart border zone of MI group, CM group, and CM + ADSC group at 4 weeks after transplantation, respectively. Scale bar = 400 μm and 100 μm, respectively. (G–H) Quantitative analysis of arteriolar (orange/green double staining cells/mm^2) and neovascular (orange staining cells/mm^2) densities in border zone of MI group, CM group, and CM + ADSC group. Results are presented as mean ± SD. Significance was determined using one-way ANOVA followed by Tukey's post hoc test. $*p < 0.05$, $**p < 0.01$, ns means no statistical significance.

organization, alignment, ECM secretion, and cytokines secretion. Furthermore, the histological findings of heart tissue samples revealed that the CM + ADSC tissue sheets have enhanced therapeutic effect in decreasing fibrosis and attenuating hypertrophy in the ischemic border zone, which is consistent with the findings on neovessels and arterial

angiogenesis (Figs. 7 and 8).

5. Conclusion

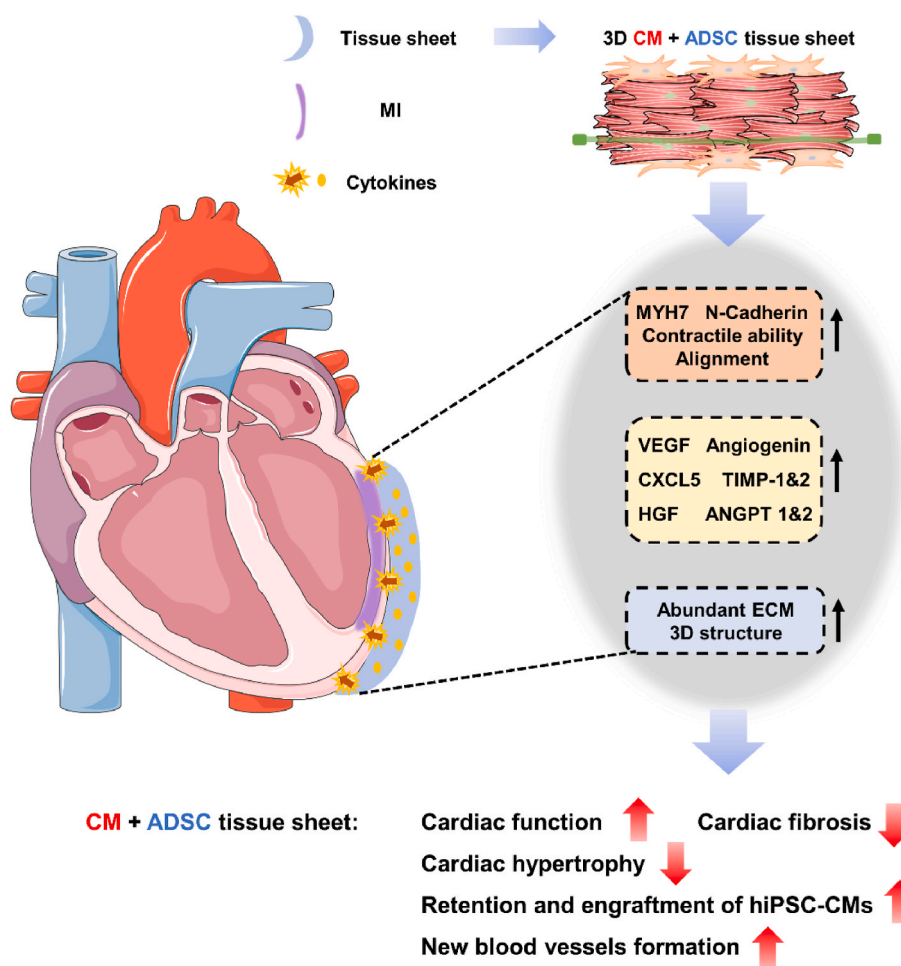In conclusion, we developed a composite, highly functional and well-

Fig. 9. Schematic diagram of the underlying mechanism of CM + ADSC tissue sheets mediated myocardial infarction therapy.

organized 3D cardiac tissue sheet using a one-step strategy. The tissue sheets exhibited improved organization, tissue thickness, alignment, ECM deposition, contractile properties, respiration function, cytokines secretion, and angiogenesis ability, while maintaining high cell viability *in vitro*. In the rat MI model, the CM + ADSC group demonstrated enhanced cardiac function recovery (4 weeks after transplantation: CM + ADSC 55.97 ± 3.06 % versus CM 46.68 ± 6.32 % [p = 0.0064] versus MI 34.89 ± 5.15 % [p = 0.0010]), augmented engraftment retention, decreased fibrosis, inhibited hypertrophy, and improved angiogenesis. Therefore, the CM + ADSC tissue sheet holds significant potential for treating ischemic heart disease.

Ethics approval and consent to participate

All procedures and protocols involving animals were approved by the ethics committee of Osaka University (approval number: 01-062-000, approval date: 2022-03-01, name of approval project: Investigation of new therapeutic effects in ischemic heart disease model animals by tissue transplantation) and were performed according to the committee's guidelines.

Consent for publication

Not applicable.

Availability of data and materials materials-methods

All data generated and/or analyzed in this study are included in this published article.

CRediT authorship contribution statement

Jingbo Zhang: Writing – review & editing, Writing – original draft, Visualization, Validation, Supervision, Software, Resources, Project administration, Methodology, Investigation, Formal analysis, Data curation, Conceptualization. **Junjun Li:** Writing – review & editing, Validation, Supervision, Software, Methodology, Funding acquisition. **Xiang Qu:** Validation, Resources, Methodology, Data curation. **Yuting Liu:** Supervision, Resources, Project administration, Methodology, Investigation. **Lifu Sun:** Validation, Supervision, Methodology. **Akima Harada:** Validation, Supervision, Methodology. **Ying Hua:** Validation, Supervision, Formal analysis, Data curation. **Nagako Sougawa:** Supervision, Resources, Data curation. **Akiko Tabata:** Software, Resources. **Li Liu:** Writing – review & editing, Validation, Supervision, Resources, Project administration, Funding acquisition, Data curation, Conceptualization. **Shigeru Miyagawa:** Supervision, Project administration, Funding acquisition.

Declaration of competing interest

The authors declare that they have no competing nonfinancial interests to declare.

Appendix A. Supplementary data

Supplementary data to this article can be found online at https://doi.org/10.1016/j.bioactmat.2024.03.028.

List of abbreviations

HF	heart failure
MI	myocardial infarction
MSC	mesenchymal stem cell
hADSC	human adipose-derived mesenchymal stem cell
VEGF	vascular endothelial growth factor
HGF	hepatocyte growth factor
PLGA	poly (lactic-*co*-glycolic acid)
ECM	extracellular matrix
LAD	left anterior descending artery
PDMS	polydimethylsiloxane
LVEF	left ventricle ejection fraction
LVFS	left ventricle fractional shortening
H&E	hematoxylin and eosin
vWF	von Willebrand Factor
α-SMA	α-smooth muscle actin

References

[1] M. Naghavi, A.A. Abajobir, C. Abbafati, K.M. Abbas, F. Abd-Allah, S.F. Abera, V. Aboyans, O. Adetokunboh, A. Afshin, A. Agrawal, W. Ahmad, M.B. Ahmed, A. N. Aichour, M.T.E. Aichour, I. Aichour, S. Aiyar, F. Alahdab, Z. Al-Aly, K. Alam, N. Alam, T. Alam, K.A. Alene, A. Al-Eyadhy, S.D. Ali, R. Alizadeh-Navaei, J. M. Alkaabi, A. Alkerwi, F. Alla, P. Allebeck, C. Allen, R. Al-Raddadi, U. Alsharif, K. A. Altirkawi, N. Alvis-Guzman, A.T. Amare, E. Amini, W. Ammar, Y.A. Amoako, N. Anber, H.H. Andersen, C.L. Andrei, S. Androudi, H. Ansari, C.A.T. Antonio, P. Anwari, J. Ärnlöv, M. Arora, A. Artaman, K.K. Aryal, H. Asayesh, S.W. Asgedom, T.M. Atey, L. Avila-Burgos, E.F.G. Avokpaho, A. Awasthi, T.K. Babalola, U. Bacha, K. Balakrishnan, A. Barac, M.A. Barboza, S.L. Barker-Collo, S. Barquera, L. Barregard, L.H. Barrero, B.T. Baune, N. Bedi, E. Beghi, Y. Béjot, B.B. Bekele, M. L. Bell, J.R. Bennett, I.M. Bensenor, A. Berhane, E. Bernabé, B.D. Betsu, M. Beuran, S. Bhatt, S. Biadgilign, K. Bienhoff, B. Bikbov, D. Bisanzio, R.R.A. Bourne, N.J. K. Breitborde, L.N.B. Bulto, B.R. Bumgarner, Z.A. Butt, L. Cahuana-Hurtado, E. Cameron, J.C. Campuzano, J. Car, R. Cárdenas, J.J. Carrero, A. Carter, D. C. Casey, C.A. Castañeda-Orjuela, F. Catalá-López, F.J. Charlson, C.E. Chibueze, O. Chimed-Ochir, V.H. Chisumpa, A.A. Chitheer, D.J. Christopher, L.G. Ciobanu, M. Cirillo, A.J. Cohen, D. Colombara, C. Cooper, B.C. Cowie, M.H. Criqui, L. Dandona, R. Dandona, P.I. Dargan, J. Das Neves, D.V. Davitoiu, K. Davletov, B. De Courten, B.K. Defo, L. Degenhardt, S. Deiparine, K. Deribe, A. Deribew, S. Dey, D. Dicker, E.L. Ding, S. Djalalinia, H.P. Do, D.T. Doku, D. Douwes-Schultz, T.R. Driscoll, M. Dubey, B.B. Duncan, M. Echko, Z.Z. El-Khatib, C.L. Ellingsen, A. Enayati, S.P. Ermakov, H.E. Erskine, S. Eskandarieh, A. Esteghamati, K. Estep, C. S.E.S. Farinha, A. Faro, F. Farzadfar, V.L. Feigin, S.-M. Fereshtehnejad, J. C. Fernandes, A.J. Ferrari, T.R. Feyissa, I. Filip, S. Finegold, F. Fischer, C. Fitzmaurice, A.D. Flaxman, N. Foigt, T. Frank, M. Fraser, N. Fullman, T. Fürst, J. M. Furtado, E. Gakidou, A.L. Garcia-Basteiro, T. Gebre, G.B. Gebregergs, T. T. Gebrehiwot, D.Y. Gebremichael, J.M. Geleijnse, R. Genova-Maleras, H. A. Gesesew, P.W. Gething, R.F. Gillum, A.Z. Giref, M. Giroud, G. Giussani, W. W. Godwin, A.L. Gold, E.M. Goldberg, P.N. Gona, S.V. Gopalani, H.N. Gouda, A. C. Goulart, M. Griswold, R. Gupta, T. Gupta, V. Gupta, P.C. Gupta, J.A. Haagsma, N. Hafezi-Nejad, A.D. Hailu, G.B. Hailu, R.R. Hamadeh, M.T. Hambisa, S. Hamidi, M. Hammami, J. Hancock, A.J. Handal, G.J. Hankey, Y. Hao, H.L. Harb, H. A. Hareri, M.S. Hassanvand, R. Havmoeller, S.I. Hay, F. He, M.T. Hedayati, N. J. Henry, I.B. Heredia-Pi, C. Herteliu, H.W. Hoek, M. Horino, N. Horita, H. D. Hosgood, S. Hostiuc, P.J. Hotez, D.G. Hoy, C. Huynh, K.M. Iburg, C. Ikeda, B. V. Ileanu, A.A. Irenso, C.M.S. Irvine, S.M.S. Islam, K.H. Jacobsen, N. Jahanmehr, M. B. Jakovljevic, M. Javanbakht, S.P. Jayaraman, P. Jeemon, V. Jha, D. John, C. O. Johnson, S.C. Johnson, J.B. Jonas, M. Jürisson, Z. Kabir, R. Kadel, A. Kahsay, R. Kamal, A. Karch, S.M. Karimi, C. Karimkhani, A. Kasaeian, N.A. Kassaw, N. J. Kassebaum, S.V. Katikireddi, N. Kawakami, P.N. Keiyoro, L. Kemmer, C. N. Kesavachandran, Y.S. Khader, E.A. Khan, Y.-H. Khang, A.T.A. Khoja, M. H. Khosravi, A. Khosravi, J. Khubchandani, A.A. Kiadaliri, C. Kieling, D. Kievlan, Y. J. Kim, D. Kim, R.W. Kimokoti, Y. Kinfu, N. Kissoon, M. Kivimaki, A.K. Knudsen, J. A. Kopec, S. Kosen, P.A. Koul, A. Koyanagi, X.R. Kulikoff, G.A. Kumar, P. Kumar, M. Kutz, H.H. Kyu, D.K. Lal, R. Lalloo, T.L.N. Lambert, Q. Lan, V.C. Lansingh, A. Larsson, P.H. Lee, J. Leigh, J. Leung, M. Levi, Y. Li, D. Li Kappe, X. Liang, M. L. Liben, S.S. Lim, P.Y. Liu, A. Liu, Y. Liu, R. Lodha, G. Logroscino, S. Lorkowski, P. A. Lotufo, R. Lozano, T.C.D. Lucas, S. Ma, E.R.K. Macarayan, E.R. Maddison, M. Magdy Abd El Razek, M. Majdan, R. Majdzadeh, A. Majeed, R. Malekzadeh, R. Malhotra, D.C. Malta, H. Manguerra, T. Manyazewal, C.C. Mapoma, L. B. Marczak, D. Markos, J. Martinez-Raga, F.R. Martins-Melo, I. Martopullo, C. McAlinden, M. McGaughey, J.J. McGrath, S. Mehata, T. Meier, K.G. Meles, P. Memiah, Z.A. Memish, M.M. Mengesha, D.T. Mengistu, B.G. Menota, G. A. Mensah, T.J. Meretoja, A. Meretoja, A. Millear, T.R. Miller, S. Minnig, M. Mirarefin, E.M. Mirrakhimov, A. Misganaw, S.R. Mishra, I.A. Mohamed, K. A. Mohammad, A. Mohammadi, S. Mohammed, A.H. Mokdad, G.L.D. Mola, S. K. Mollenkopf, M. Molokhia, L. Monasta, J.C. Montañez, M. Montico, M. D. Mooney, M. Moradi-Lakeh, P. Moraga, L. Morawska, C. Morozoff, S.D. Morrison, C. Mountjoy-Venning, K.B. Mruts, K. Muller, G.V.S. Murthy, K.I. Musa, J. B. Nachega, A. Naheed, L. Naldi, V. Nangia, B.R. Nascimento, J.T. Nasher, G. Natarajan, I. Negoi, J.W. Ngunjiri, C.T. Nguyen, Q.L. Nguyen, T.H. Nguyen, G. Nguyen, M. Nguyen, E. Nichols, D.N.A. Ningrum, V.M. Nong, J.J.N. Noubiap, F. A. Ogbo, I.-H. Oh, A. Okoro, A.T. Olagunju, H.E. Olsen, B.O. Olusanya, J. O. Olusanya, K. Ong, J.N. Opio, E. Oren, A. Ortiz, M. Osman, E. Ota, M. Pa, R. E. Pacella, S. Pakhale, A. Pana, B.K. Panda, S. Panda-Jonas, C. Papachristou, E.- K. Park, S.B. Patten, G.C. Patton, D. Paudel, K. Paulson, D.M. Pereira, F. Perez-Ruiz, N. Perico, A. Pervaiz, M. Petzold, M.R. Phillips, D.M. Pigott, C. Pinho, D. Plass, M. A. Pletcher, S. Polinder, M.J. Postma, F. Pourmalek, C. Purcell, M. Qorbani, B.P. A. Quintanilla, A. Radfar, A. Rafay, V. Rahimi-Movaghar, M.H.U. Rahman, M. Rahman, R.K. Rai, C.L. Ranabhat, Z. Rankin, P.C. Rao, G.K. Rath, S. Rawaf, S. E. Ray, J. Rehm, R.C. Reiner, M.B. Reitsma, G. Remuzzi, S. Rezaei, M.S. Rezai, M. B. Rokni, L. Ronfani, G. Roshandel, G.A. Roth, D. Rothenbacher, G.M. Ruhago, R. Sa, S. Saadat, P.S. Sachdev, N. Sadat, M. Safdarian, S. Safi, S. Safiri, R. Sagar, R. Sahathevan, J. Salama, P. Salamati, J.A. Salomon, A.M. Samy, J.R. Sanabria, M. D. Sanchez-Niño, D. Santomauro, I.S. Santos, M.M. Santric Milicevic, B. Sartorius, M. Satpathy, M.I. Schmidt, I.J.C. Schneider, S. Schulhofer-Wohl, A.E. Schutte, D. C. Schwebel, F. Schwendicke, S.G. Sepanlou, E.E. Servan-Mori, K.A. Shackelford, S. Shahraz, M.A. Shaikh, M. Shamsipour, M. Shamsizadeh, J. Sharma, R. Sharma, J. She, S. Sheikhbahaei, M. Shey, P. Shi, C. Shields, M. Shigematsu, R. Shiri, S. Shirude, I. Shiue, H. Shoman, M.G. Shrime, I.D. Sigfusdottir, N. Silpakit, J. P. Silva, J.A. Singh, A. Singh, E. Skiadaresi, A. Sligar, D.L. Smith, A. Smith, M. Smith, B.H.A. Sobaih, S. Soneji, R.J.D. Sorensen, J.B. Soriano, C. T. Sreeramareddy, V. Srinivasan, J.D. Stanaway, V. Stathopoulou, N. Steel, D. J. Stein, C. Steiner, S. Steinke, M.A. Stokes, M. Strong, B. Strub, M. Subart, M. B. Sufiyan, B.F. Sunguya, P.J. Sur, S. Swaminathan, B.L. Sykes, R. Tabarés-Seisdedos, S.K. Tadakamalla, K. Takahashi, J.S. Takala, R.T. Talongwa, M. R. Tarawneh, M. Tavakkoli, N. Taveira, T.K. Tegegne, A. Tehrani-Banihashemi, M.- H. Temsah, A.S. Terkawi, J.S. Thakur, O. Thamsuwan, K.R. Thankappan, K. E. Thomas, A.H. Thompson, A.J. Thomson, A.G. Thrift, R. Tobe-Gai, R. Topor-Madry, A. Torre, M. Tortajada, J.A. Towbin, B.X. Tran, C. Troeger, T. Truelsen, D. Tsoi, E.M. Tuzcu, S. Tyrovolas, K.N. Ukwaja, E.A. Undurraga, R. Updike, O. A. Uthman, B.S.C. Uzochukwu, J.F.M. Van Boven, T. Vasankari, N. Venketasubramanian, F.S. Violante, V.V. Vlassov, S.E. Vollset, T. Vos, T. Wakayo, M.T. Wallin, Y.-P. Wang, E. Weiderpass, R.G. Weintraub, D.J. Weiss, A. Werdecker, R. Westerman, B. Whetter, H.A. Whiteford, T. Wijeratne, C. S. Wiysonge, B.G. Woldeyes, C.D.A. Wolfe, R. Woodbrook, A. Workicho, D. Xavier, Q. Xiao, G. Xu, M. Yaghoubi, B. Yakob, Y. Yano, M. Yaseri, H.H. Yimam, N. Yonemoto, S.-J. Yoon, M. Yotebieng, M.Z. Younis, Z. Zaidi, M.E.S. Zaki, E. A. Zegeye, Z.M. Zenebe, T.A. Zerfu, A.L. Zhang, X. Zhang, B. Zipkin, S. Zodpey, A. D. Lopez, C.J.L. Murray, Global, regional, and national age-sex specific mortality for 264 causes of death, 1980–2016: a systematic analysis for the Global Burden of Disease Study 2016, Lancet 390 (2017) 1151–1210, https://doi.org/10.1016/S0140-6736(17)32152-9.

[2] S.S. Virani, A. Alonso, H.J. Aparicio, E.J. Benjamin, M.S. Bittencourt, C. W. Callaway, A.P. Carson, A.M. Chamberlain, S. Cheng, F.N. Delling, M.S.V. Elkind, K.R. Evenson, J.F. Ferguson, D.K. Gupta, S.S. Khan, B.M. Kissela, K.L. Knutson, C. D. Lee, T.T. Lewis, J. Liu, M.S. Loop, P.L. Lutsey, J. Ma, J. Mackey, S.S. Martin, D. B. Matchar, M.E. Mussolino, S.D. Navaneethan, A.M. Perak, G.A. Roth, Z. Samad, G.M. Satou, E.B. Schroeder, S.H. Shah, C.M. Shay, A. Stokes, L.B. VanWagner, N.- Y. Wang, C.W. Tsao, On behalf of the American heart association council on epidemiology and prevention statistics committee and stroke statistics subcommittee, heart disease and stroke statistics—2021 update: a report from the American heart association, Circulation 143 (2021), https://doi.org/10.1161/CIR.0000000000000950.

[3] S.E. Senyo, M.L. Steinhauser, C.L. Pizzimenti, V.K. Yang, L. Cai, M. Wang, T.- D. Wu, J.-L. Guerquin-Kern, C.P. Lechene, R.T. Lee, Mammalian heart renewal by pre-existing cardiomyocytes, Nature 493 (2013) 433–436, https://doi.org/10.1038/nature11682.

[4] R. Guo, F. Wan, M. Morimatsu, Q. Xu, T. Feng, H. Yang, Y. Gong, S. Ma, Y. Chang, S. Zhang, Y. Jiang, H. Wang, D. Chang, H. Zhang, Y. Ling, F. Lan, Cell sheet formation enhances the therapeutic effects of human umbilical cord mesenchymal stem cells on myocardial infarction as a bioactive material, Bioact. Mater. 6 (2021) 2999–3012, https://doi.org/10.1016/j.bioactmat.2021.01.036.

[5] H. Hashimoto, E.N. Olson, R. Bassel-Duby, Therapeutic approaches for cardiac regeneration and repair, Nat. Rev. Cardiol. 15 (2018) 585–600, https://doi.org/10.1038/s41569-018-0036-6.

[6] Y. Shiba, T. Gomibuchi, T. Seto, Y. Wada, H. Ichimura, Y. Tanaka, T. Ogasawara, K. Okada, N. Shiba, K. Sakamoto, D. Ido, T. Shiina, M. Ohkura, J. Nakai, N. Uno, Y. Kazuki, M. Oshimura, I. Minami, U. Ikeda, Allogeneic transplantation of iPS cell-derived cardiomyocytes regenerates primate hearts, Nature 538 (2016) 388–391, https://doi.org/10.1038/nature19815.

[7] A. Ghiroldi, M. Piccoli, F. Cirillo, M.M. Monasky, G. Ciconte, C. Pappone, L. Anastasia, Cell-based therapies for cardiac regeneration: a comprehensive review of past and ongoing strategies, Int. J. Mol. Sci. 19 (2018) 3194, https://doi.org/10.3390/ijms19103194.

[8] O. Pfister, G. Della Verde, R. Liao, G.M. Kuster, Regenerative therapy for cardiovascular disease, Transl. Res. 163 (2014) 307–320, https://doi.org/10.1016/j.trsl.2013.12.005.

[9] K.H. Schuleri, G.S. Feigenbaum, M. Centola, E.S. Weiss, J.M. Zimmet, J. Turney, J. Kellner, M.M. Zviman, K.E. Hatzistergos, B. Detrick, J.V. Conte, I. McNiece, C. Steenbergen, A.C. Lardo, J.M. Hare, Autologous mesenchymal stem cells produce reverse remodelling in chronic ischaemic cardiomyopathy, Eur. Heart J. 30 (2009) 2722–2732, https://doi.org/10.1093/eurheartj/ehp265.

[10] S. Liao, Y. Zhang, S. Ting, Z. Zhen, F. Luo, Z. Zhu, Y. Jiang, S. Sun, W.-H. Lai, Q. Lian, H.-F. Tse, Potent immunomodulation and angiogenic effects of mesenchymal stem cells versus cardiomyocytes derived from pluripotent stem cells for treatment of heart failure, Stem Cell Res. Ther. 10 (2019) 78, https://doi.org/10.1186/s13287-019-1183-3.

[11] M.E. Bernardo, W.E. Fibbe, Mesenchymal stromal cells: sensors and switchers of inflammation, Cell Stem Cell 13 (2013) 392–402, https://doi.org/10.1016/j.stem.2013.09.006.

[12] T. Ma, J. Sun, Z. Zhao, W. Lei, Y. Chen, X. Wang, J. Yang, Z. Shen, A brief review: adipose-derived stem cells and their therapeutic potential in cardiovascular diseases, Stem Cell Res. Ther. 8 (2017) 124, https://doi.org/10.1186/s13287-017-0585-3.

[13] J. Zhang, J. Li, X. Qu, Y. Liu, A. Harada, Y. Hua, N. Yoshida, M. Ishida, A. Tabata, L. Sun, L. Liu, S. Miyagawa, Development of a thick and functional human adipose-derived stem cell tissue sheet for myocardial infarction repair in rat hearts, Stem Cell Res. Ther. 14 (2023) 380, https://doi.org/10.1186/s13287-023-03560-9.

[14] Y. Xia, X. Xu, Y. Guo, C. Lin, X. Xu, F. Zhang, M. Fan, T. Qi, C. Li, G. Hu, L. Peng, S. Wang, L. Zhang, C. Hai, R. Liu, W. Yan, L. Tao, Mesenchymal stromal cells overexpressing farnesoid X receptor exert cardioprotective effects against acute ischemic heart injury by binding endogenous bile acids, Adv. Sci. 9 (2022) e2200431, https://doi.org/10.1002/advs.202200431.

[15] R. Wu, X. Hu, J. Wang, Concise review: optimized strategies for stem cell-based therapy in myocardial repair: clinical translatability and potential limitation, Stem Cell. 36 (2018) 482–500, https://doi.org/10.1002/stem.2778.

[16] J. Li, X. Qu, L. Liu, L. Li, Y. Hua, J. Zhang, M. Ishida, N. Yoshida, A. Tabata, N. Sougawa, E. Ito, N. Mochizuki-Oda, A. Harada, T. Kawamura, R. Matsuura, Y. Wang, K. Morishima, S. Miyagawa, Y. Sawa, Developing thick cardiac tissue with a multilayer fiber sheet for treating myocardial infarction, Adv. Fiber Mater. (2023), https://doi.org/10.1007/s42765-023-00313-4.

[17] J. Li, I. Minami, M. Shiozaki, L. Yu, S. Yajima, S. Miyagawa, Y. Shiba, N. Morone, S. Fukushima, M. Yoshioka, S. Li, J. Qiao, X. Li, L. Wang, H. Kotera, N. Nakatsuji, Y. Sawa, Y. Chen, L. Liu, Human pluripotent stem cell-derived cardiac tissue-like constructs for repairing the infarcted myocardium, Stem Cell Rep. 9 (2017) 1546–1559, https://doi.org/10.1016/j.stemcr.2017.09.007.

[18] X. Qu, J. Li, L. Liu, J. Zhang, Y. Hua, K. Suzuki, A. Harada, M. Ishida, N. Yoshida, D. Okuzaki, Y. Sakai, Y. Sawa, S. Miyagawa, ONO-1301 enhances post-transplantation survival of human induced pluripotent stem cell-derived cardiac tissue sheet by promoting angiogenesis, J. Heart Lung Transplant. 42 (2023) 716–729, https://doi.org/10.1016/j.healun.2023.01.018.

[19] K. Suzuki, S. Miyagawa, L. Liu, T. Kawamura, J. Li, X. Qu, A. Harada, K. Toda, D. Yoshioka, S. Kainuma, A. Kawamura, Y. Sawa, Therapeutic efficacy of large aligned cardiac tissue derived from induced pluripotent stem cell in a porcine ischemic cardiomyopathy model, J. Heart Lung Transplant. 40 (2021) 767–777, https://doi.org/10.1016/j.healun.2021.04.010.

[20] T. Nakazato, T. Kawamura, T. Uemura, L. Liu, J. Li, M. Sasai, A. Harada, E. Ito, H. Iseoka, K. Toda, Y. Sawa, S. Miyagawa, Engineered three-dimensional cardiac tissues maturing in a rotating wall vessel bioreactor remodel diseased hearts in rats with myocardial infarction, Stem Cell Rep. 17 (2022) 1170–1182, https://doi.org/10.1016/j.stemcr.2022.03.012.

[21] Y.-W. Liu, B. Chen, X. Yang, J.A. Fugate, F.A. Kalucki, A. Futakuchi-Tsuchida, L. Couture, K.W. Vogel, C.A. Astley, A. Baldessari, J. Ogle, C.W. Don, Z. L. Steinberg, S.P. Seslar, S.A. Tuck, H. Tsuchida, A.V. Naumova, S.K. Dupras, M. S. Lyu, J. Lee, D.W. Hailey, H. Reinecke, L. Pabon, B.H. Fryer, W.R. MacLellan, R. S. Thies, C.E. Murry, Human embryonic stem cell-derived cardiomyocytes restore function in infarcted hearts of non-human primates, Nat. Biotechnol. 36 (2018) 597–605, https://doi.org/10.1038/nbt.4162.

[22] J. Li, L. Liu, J. Zhang, X. Qu, T. Kawamura, S. Miyagawa, Y. Sawa, Engineered tissue for cardiac regeneration: current status and future perspectives, Bioengineering 9 (2022) 605, https://doi.org/10.3390/bioengineering9110605.

[23] P. Gentile, V. Chiono, I. Carmagnola, P. Hatton, An overview of poly(lactic-co-glycolic) acid (PLGA)-Based, Biomater. Bone Tissue Eng., IJMS 15 (2014) 3640–3659, https://doi.org/10.3390/ijms15033640.

[24] S.R. Abulateefeh, Long-acting injectable PLGA/PLA depots for leuprolide acetate: successful translation from bench to clinic, Drug Deliv. Transl. Res. 13 (2023) 520–530, https://doi.org/10.1007/s13346-022-01228-0.

[25] J. Zhang, X. Qu, J. Li, A. Harada, Y. Hua, N. Yoshida, M. Ishida, Y. Sawa, L. Liu, S. Miyagawa, Tissue sheet engineered using human umbilical cord-derived mesenchymal stem cells improves diabetic wound healing, Indian J. Manag. Sci. 23 (2022) 12697, https://doi.org/10.3390/ijms232012697.

[26] S. Yoshida, S. Miyagawa, S. Fukushima, T. Kawamura, N. Kashiyama, F. Ohashi, T. Toyofuku, K. Toda, Y. Sawa, Maturation of human induced pluripotent stem cell-derived cardiomyocytes by soluble factors from human mesenchymal stem cells, Mol. Ther. 26 (2018) 2681–2695, https://doi.org/10.1016/j.ymthe.2018.08.012.

[27] T.B. Rogers, S. Pati, S. Gaa, D. Riley, A.Y. Khakoo, S. Patel, R.D. Wardlow, C. A. Frederick, G. Hall, L.-P. He, W.J. Lederer, Mesenchymal stem cells stimulate protective genetic reprogramming of injured cardiac ventricular myocytes, J. Mol. Cell. Cardiol. 50 (2011) 346–356, https://doi.org/10.1016/j.yjmcc.2010.09.001.

[28] S. Yoshida, S. Miyagawa, T. Toyofuku, S. Fukushima, T. Kawamura, A. Kawamura, N. Kashiyama, Y. Nakamura, K. Toda, Y. Sawa, Syngeneic mesenchymal stem cells reduce immune rejection after induced pluripotent stem cell-derived allogeneic cardiomyocyte transplantation, Sci. Rep. 10 (2020) 4593, https://doi.org/10.1038/s41598-020-58126-z.

[29] I. Arnaoutova, H.K. Kleinman, In vitro angiogenesis: endothelial cell tube formation on gelled basement membrane extract, Nat. Protoc. 5 (2010) 628–635, https://doi.org/10.1038/nprot.2010.6.

[30] G. Carpentier, S. Berndt, S. Ferratge, W. Rasband, M. Cuendet, G. Uzan, P. Albanese, Angiogenesis analyzer for ImageJ — a comparative morphometric analysis of "endothelial tube formation assay" and "fibrin bead assay,", Sci. Rep. 10 (2020) 11568 https://doi.org/10.1038/s41598-020-67289-8.

[31] J. Yokoyama, S. Miyagawa, T. Akagi, M. Akashi, Y. Sawa, Human induced pluripotent stem cell-derived three-dimensional cardiomyocyte tissues ameliorate the rat ischemic myocardium by remodeling the extracellular matrix and cardiac protein phenotype, PLoS One 16 (2021) e0245571, https://doi.org/10.1371/journal.pone.0245571.

[32] B.A. Tompkins, W. Balkan, J. Winkler, M. Gyöngyösi, G. Goliasch, F. Fernández-Avilés, J.M. Hare, Preclinical studies of stem cell therapy for heart disease, Circ. Res. 122 (2018) 1006–1020, https://doi.org/10.1161/CIRCRESAHA.117.312486.

[33] E.M. Elmowafy, M. Tiboni, M.E. Soliman, Biocompatibility, biodegradation and biomedical applications of poly(lactic acid)/poly(lactic-co-glycolic acid) micro and nanoparticles, J. Pharm. Invest. 49 (2019) 347–380, https://doi.org/10.1007/s40005-019-00439-x.

[34] M. Kawamura, S. Miyagawa, K. Miki, A. Saito, S. Fukushima, T. Higuchi, T. Kawamura, T. Kuratani, T. Daimon, T. Shimizu, T. Okano, Y. Sawa, Feasibility, safety, and therapeutic efficacy of human induced pluripotent stem cell-derived cardiomyocyte sheets in a porcine ischemic cardiomyopathy model, Circulation 126 (2012), https://doi.org/10.1161/CIRCULATIONAHA.111.084343.

[35] K. Neef, F. Drey, V. Lepperhof, T. Wahlers, J. Hescheler, Y.-H. Choi, T. Šarić, Co-Transplantation of mesenchymal stromal cells and induced pluripotent stem cell-derived cardiomyocytes improves cardiac function after myocardial damage, Front. Cardiovasc. Med. 8 (2022) 794690, https://doi.org/10.3389/fcvm.2021.794690.

[36] J.H. Houtgraaf, W.K. Den Dekker, B.M. Van Dalen, T. Springeling, R. De Jong, R. J. Van Geuns, M.L. Geleijnse, F. Fernandez-Aviles, F. Zijlsta, P.W. Serruys, H. J. Duckers, First experience in humans using adipose tissue–derived regenerative cells in the treatment of patients with ST-segment elevation myocardial infarction, J. Am. Coll. Cardiol. 59 (2012) 539–540, https://doi.org/10.1016/j.jacc.2011.09.065.

[37] E. Przybyt, M.J.A. Van Luyn, M.C. Harmsen, Extracellular matrix components of adipose derived stromal cells promote alignment, organization, and maturation of cardiomyocytes *in vitro*, J. Biomed. Mater. Res. 103 (2015) 1840–1848, https://doi.org/10.1002/jbm.a.35311.

[38] H. Xing, H. Lee, L. Luo, T.R. Kyriakides, Extracellular matrix-derived biomaterials in engineering cell function, Biotechnol. Adv. 42 (2020) 107421, https://doi.org/10.1016/j.biotechadv.2019.107421.

[39] X. Lou, Y. Tang, L. Ye, D. Pretorius, V.G. Fast, A.M. Kahn-Krell, J. Zhang, J. Zhang, A. Qiao, G. Qin, T. Kamp, J.A. Thomson, J. Zhang, Cardiac muscle patches containing four types of cardiac cells derived from human pluripotent stem cells improve recovery from cardiac injury in mice, Cardiovasc. Res. 119 (2023) 1062–1076, https://doi.org/10.1093/cvr/cvad004.

[40] M. Gnecchi, H. He, O.D. Liang, L.G. Melo, F. Morello, H. Mu, N. Noiseux, L. Zhang, R.E. Pratt, J.S. Ingwall, V.J. Dzau, Paracrine action accounts for marked protection of ischemic heart by Akt-modified mesenchymal stem cells, Nat. Med. 11 (2005) 367–368, https://doi.org/10.1038/nm0405-367.